



***Facultad
de
Ciencias***

**Analysis and numerical simulation of
mooring lines in complex bathymetries
(Análisis y simulación numérica de líneas de
fondeo en batimetrías complejas)**

Trabajo de Fin de Grado
para acceder al

GRADO EN MATEMÁTICAS

Autora: Paula Desiré Valdor

Director: Luis Alberto Fernández Fernández

Co-Director: Álvaro Rodríguez Luis

Junio - 2022

Me gustaría dar las gracias a Luis Alberto por todo el tiempo y esfuerzo que ha invertido en este trabajo, por ofrecer su ayuda en todo momento.

Quiero agradecer a Álvaro toda la dedicación y entusiasmo que ha puesto en este proyecto: gracias por darme una visión distinta, pero a la vez tan interesante de las matemáticas. También me gustaría agradecer al grupo de ingeniería offshore del IHCantabria el trato tan amable y cercano que he recibido trabajando con ellos el pasado verano.

Por último, gracias también a todos los que me han acompañado en esta etapa, a mi familia y a mis compañeros. Con vuestra ayuda, todo ha sido más fácil.

Resumen

Las líneas de fondeo sujetan las estructuras flotantes que se colocan en alta mar, soportando así grandes tensiones producidas por dispositivos muy pesados siguiendo los movimientos de las olas. Esto puede llevar al deterioro de las líneas e incluso a la pérdida del dispositivo. Para evitar estas situaciones, se simula el comportamiento de las líneas de fondeo con toda la precisión posible, lo que motiva a considerar la interacción de la línea con el fondo marino de forma muy precisa.

El objetivo de este TFG es diseñar e implementar un algoritmo capaz de simular las líneas de fondeo incluyendo su interacción con un fondo marino descrito por batimetrías complejas. Para ello, se han estudiado las ecuaciones en derivadas parciales que definen la dinámica de las líneas de fondeo. Posteriormente, se ha encontrado una solución analítica para un caso bidimensional estático con una configuración particular y por último, se ha resuelto el caso genérico tridimensional de forma numérica utilizando el método de elementos finitos.

Para poder considerar la interacción con el fondo de forma genérica en la simulación numérica, se ha desarrollado un nuevo algoritmo continuo de proyección que opera de forma eficiente dependiendo del tipo de fondo marino: en los casos en los que es horizontal o tiene forma de plano inclinado basta con utilizar un método directo de proyección mientras que, en fondos irregulares, se contruye una triangulación que describe el suelo y se realiza un proceso de proyección óptimo basado en las normales de vértice. La utilización de este algoritmo permite calcular con precisión las fuerzas de fricción y normales a las que está sujeta la línea, mejorando su simulación.

Finalmente, la situación particular resuelta analíticamente se ha resuelto también de forma numérica, encontrando un acuerdo excelente entre los resultados de ambos métodos: las diferencias relativas entre las posiciones obtenidas de las líneas de fondeo son del orden del 0.01% mientras que las discrepancias en las tensiones en la parte final de la línea son inferiores al 0.1%. También se ha analizado la posición de la línea simulada numéricamente en varios fondos marinos descritos por batimetrías complejas.

Palabras clave: Líneas de fondeo, método de elementos finitos, batimetría compleja, algoritmo continuo de proyección.

Abstract

Mooring lines secure offshore floating structures, withstanding high stresses produced by very heavy devices following wave movements. This can lead to the deterioration of the lines and even to the loss of the device. To avoid these situations, the behavior of the mooring lines is simulated with all the possible precision, which leads to consider the interaction of the line with the seafloor.

The objective of this work is to develop and implement an algorithm able to simulate mooring lines including its interaction with a seabed described by complex bathymetries. The first step is to study the system of partial differential equations that define the dynamic behaviour of the mooring lines. Later, a two-dimensional static case with a particular configuration will be solved analytically. Then, the generic three-dimensional case will be solved numerically using the finite element method.

In order to consider the interaction with the seabed, a new continuous projection algorithm will be developed. The constructed algorithm operates efficiently depending on the type of seabed: in cases where it is flat (horizontal or inclined plane), a direct projection method can be used while, in an irregular seafloor, the seabed is described by a triangulation and an optimal projection process based on the vertex normals is performed. The use of this algorithm allows to accurately calculate the friction and normal forces on the mooring line, improving its simulation.

Finally, the particular situation solved analytically will also be solved numerically, finding an excellent agreement between both methods: the relative differences between them of the order of a 0.01% for the obtained mooring line positions and less than 0.1% for the tensions at the line endpoint. In addition, several qualitative tests which studied the numerically obtained mooring line positioning in complex bathymetries were performed.

Keywords: Mooring lines, finite element method, complex bathymetry, continuous projection algorithm.

Contents

1	Introduction	4
2	Formulation of the problem	6
2.1	General formulation	6
2.2	Wave type equation formulation	7
2.3	Brief description a more complex model	8
3	Bidimensional specific case: Mooring in a slope	9
3.1	Description of the specific static case	9
3.2	Analytical resolution	10
3.2.1	Deduction of catenary equation	10
3.2.2	Parameterization of the catenary part	12
3.2.3	Parameterization of the part which lays on the slope	13
3.2.4	Determination of l_0	14
3.2.5	Final solution	15
3.2.6	Verification of the obtained expressions	15
4	Three dimensional general case	17
4.1	Numerical method (FEM)	17
4.1.1	Homogenization of the problem	18
4.1.2	Weak formulation	19
4.1.3	Discretization/ Galerkin continuous method	20
4.1.4	Definition of the basis	21
4.1.5	From second order to first order ODEs system	22
4.2	Continuous projection algorithm	23
4.2.1	Definition of the terms	23
4.2.2	Specific cases: Horizontal or inclined plane seabed surface	24
4.2.3	General case: Complex bathymetry	25
4.2.4	Application: Calculation of ground normal and friction forces.	29
4.3	Initial condition problem: Newton-Armijo	32
5	Results	35
5.1	Comparison between the analytic and simulation results	35
5.1.1	Tension at the fairlead comparison	36
5.1.2	Position comparison	37
5.2	Qualitative tests	38
6	Conclusions	41
7	Additional work	43
	References	47

1 Introduction

The development of renewable energy is one of the most important global issues today, as it would be an alternative to the burning of fossil fuels that is causing global warming. Therefore, a lot of money and effort is being invested in the study of clean energy sources, including wind and wave power. The latter two can be efficiently exploited in deep water areas by installing floating structures able to obtain electrical energy such as wind turbines or wave energy converters.

The floating structures are secured by mooring systems commonly formed by several mooring lines. A line is anchored to the seabed and ends in a point commonly located in the sea surface called the fairlead, which in general is non-static and follows the wave movement. The mooring line is constantly slacked and retightened by the wave, and it often holds very heavy devices, imposing high peak tensions in the mooring line that can easily cause it to break. However, a failure in mooring systems may cause a damage or even a loss of the device, resulting in a severe economic loss. In fact, Kempener and Neumann (2014) list moorings as a main priority in wave energy research and development.

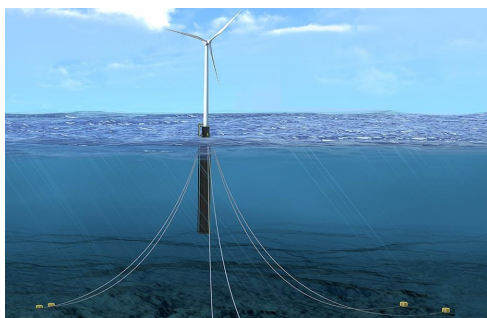


Figure 1: A mooring system composed of several mooring lines securing a wind floating turbine.

In order to reproduce with precision and improve the behavior and response of mooring lines, numerical simulations which imitate its dynamics are developed. Most of them are based on finite element method (Aamo and Fossen, 2000; Montano et al., 2007).

Gobat and Grosenbaugh (2001) concluded in his work that the seabed interaction affects the tensions to which the mooring line is subjected. In addition, when the mooring line dynamics is evaluated, friction and ground normal forces should be accurately described, as both of them depend on the seabed surface. Nevertheless, the modelization of a floor distinct from an horizontal one has barely been studied, introducing errors and worsening the numerical simulations results. In addition, the error caused by this approximation even worsens at deep waters, where the seabed usually describes more sloped configurations, which are the common depths to install mooring devices. For instance, there are certain locations such as the Canary Islands where the seafloor is commonly described by several irregularities.

There are certain previously developed models which consider the mooring line interaction with a seafloor surface distinct from an horizontal plane such as the two dimensional static numerical model of a mooring line in a slope developed by Feng et al. (2020). There are also

three commercial software tools able to simulate mooring lines in irregular bathymetries: *OrcaFlex*, *ProteusDS* and *FlexCom*. In the manual of *Orcaflex* (Orcaflex, 1987-2022) it is explained that the seabed coordinates are used to construct a triangulation which is interpolated by either a linear or a cubic polynomial method, while *FlexCom*, as it is stated in its manual (Flexcom, 2021), is also based on a cubic interpolation method of the triangulation. *ProteusDS* software (ProteusDS, 2018) uses a mesh discretized into squares describing the seabed equipped with polygonal normals able to model ground normal and friction forces. Nevertheless, there is a gap in literature because none of the above methods are described in detail.

The aim of this work is to equip the already developed mooring lines numerical model at *IHCantabria* (Rodríguez et al., 2020) with a new developed tool able to evaluate the seabed interaction. The tool is based on a state of the art continuous projection method (Orazi and Reggiani, 2020) which describes the projection surface by a triangulation and uses vertex normals to project. The developed projection method is capable of interpreting any seabed configuration and of calculating friction and ground normal forces. This will allow to simulate numerically a mooring line in a complex bathymetry.

This work is divided as follows: it starts with the mathematical formulation of the mooring line dynamics, shown in section 2. Then, in section 3, the mooring is described in two dimensions and a particular static configuration in which an analytical solution can be constructed, is studied. In section 4, the mooring line is studied in a three dimensional frame. This time, the line is no longer static and the solution must be found numerically. The section starts with a brief description of the finite element method used to solve the system and then describes the continuous projection method developed to evaluate seabed interaction and its application to the calculation of friction and ground forces. The last part of the section studies how Newton-Armijo was used to search for the initial condition needed to solve the problem. Finally, in section 5 the analytic results were compared with the ones obtained numerically providing an excellent accordance. In addition, the results of some qualitative tests are shown, demonstrating the ability of the simulation to model a mooring line in a complex bathymetry. The work ends up with some conclusions and an analysis of the possible further research in section 6.

2 Formulation of the problem

The objective is to describe the mooring line positions along the time. The mooring dynamics description will depend on the time variable t and on the arc length parameter s , with $s \in [0, L]$ being L the mooring length. The mooring line changes its positions, velocities and accelerations with time because its fairlead moves following a vector that must be provided.

It is widely common to describe mooring lines in both two or three dimensions. The three dimensional description is the natural approach, but it is also habitual to see descriptions in two dimensions, as lines are much longer than wide, allowing to use a two dimensional frame which describes the mooring line length and the depth it is submerged into. Therefore, the equations in this section will be introduced in a variable dimensional environment \mathbb{R}^n . However, the only values n can take are $n \in \{2, 3\}$. In section 3, the mooring will be described in a two dimensional frame while in section 4, three dimensions will be considered.

From now on, the vectors will be written in bold characters and all the points will be described by its three coordinate vector position.

2.1 General formulation

A mooring line behaviour can be modelled by Newton's equation expressed per unit of length:

$$\gamma_0 \frac{\partial^2 \mathbf{r}(t, s)}{\partial t^2} = \frac{\partial}{\partial s} \left(T(t, s) \frac{\partial \mathbf{r}(t, s)}{\partial s} \right) + \mathbf{f}(t, s) \quad (1)$$

where γ_0 is the mooring line mass per meter, $\mathbf{r} : [0, \infty) \times [0, L] \rightarrow \mathbb{R}^n$ is the position of the mooring, $T : [0, \infty) \times [0, L] \rightarrow \mathbb{R}$ is the mooring tension, $\frac{\partial \mathbf{r}}{\partial s} : [0, \infty) \times [0, L] \rightarrow \mathbb{R}^n$ is the unitary tangential vector to the mooring and $\mathbf{f} : [0, \infty) \times [0, L] \rightarrow \mathbb{R}^n$ is the external forces vector. This formulation is based on Palm et al. (2013) model, and is a simplification of a more complex model which has been briefly described in subsection 2.3.

The external forces vector $\mathbf{f}(t, s)$ per unit of length is the sum of the

$$\mathbf{f}(t, s) = \mathbf{f}_{bg}(t, s) + \mathbf{f}_d(t, s) + \mathbf{f}_{am}(t, s) + \mathbf{f}_n(t, s) + \mathbf{f}_f(t, s) \quad (2)$$

being

- $\mathbf{f}_{bg}(t, s)$ Effective weight, which is the resultant between the buoyancy and weight forces obtained by applying Archimedes Principle. It always appears, as the mooring line is always submerged in the sea water.
- $\mathbf{f}_d(t, s)$ Hydrodynamic drag force, which appears when the mooring line is not static and opposes the mooring line motion through the water.
- $\mathbf{f}_{am}(t, s)$ Added mass force, which models the displacement of fluid caused by the mooring line motion.
- $\mathbf{f}_n(t, s)$ Ground normal force, which must be taken into account when the mooring is in contact with the seabed. Its direction is perpendicular to the seabed surface. Its modeling depends on the seafloor surface and has been described in Eq.(24).

- $\mathbf{f}_f(t, s)$ Friction force, which has to be considered when the mooring line touches the seafloor. Its direction is contained in the seabed surface plane, and therefore, depends on it. Its description can be seen in Eq.(25).

The description of the model used for each of these forces extends beyond the limits of this work, but it is detailed in Desiré et al. (2022). All of them are treated as forces per unit of length.

Eq.(1) describes a PDE System, with n equations. In addition, the problem is restricted to certain conditions:

- The spatial boundaries are imposed by the anchor and fairlead: the anchor is fixed to a point \mathbf{r}_0 and the fairlead position is described by the provided vector which depends on time $\mathbf{r}_F : [0, \infty) \rightarrow \mathbb{R}^n$:

$$\mathbf{r}(t, 0) = \mathbf{r}_0 ; \mathbf{r}(t, L) = \mathbf{r}_F(t)$$

The fairlead vector is usually described by a sinusoidal equation, imitating the wave movement.

- The problem is described by certain initial conditions ($t = 0$) in the mooring line. As Eq.(1) depends on second derivatives, the initial mooring line position $\mathbf{r}(0, s)$ and velocity $\frac{\partial \mathbf{r}(0, s)}{\partial t}$ must be provided in order to solve the system. The initial mooring line velocity will be considered zero while the initial mooring line position will be described by a function $\mathbf{g}(s)$.

$$\frac{\partial \mathbf{r}(0, s)}{\partial t} = \mathbf{0} ; \mathbf{r}(0, s) = \mathbf{g}(s)$$

Previous considerations let express the problem as follows:

$$\left\{ \begin{array}{ll} \gamma_0 \frac{\partial^2 \mathbf{r}(t, s)}{\partial t^2} = \frac{\partial}{\partial s} \left(T(t, s) \frac{\partial \mathbf{r}(t, s)}{\partial s} \right) + \mathbf{f}(t, s) & \text{if } s \in (0, L), t > 0 & \text{PDE system} \\ \mathbf{r}(t, 0) = \mathbf{r}_0 & \text{if } t > 0 & \text{Boundary conditions} \\ \mathbf{r}(t, L) = \mathbf{r}_F(t) & \text{if } t > 0 & \\ \mathbf{r}(0, s) = \mathbf{g}(s) & \text{if } s \in (0, L) & \text{Initial conditions} \\ \frac{\partial \mathbf{r}(0, s)}{\partial t} = \mathbf{0} & \text{if } s \in (0, L) & \end{array} \right. \quad (3)$$

In this work, a particular static case of the mooring will be discussed in section 3, which will allow to find an analytic solution for the system of PDEs obtained. However, resolving the non-static equation in general is complicated and precises to use numerical methods. This other perspective will be discussed in section 4.

2.2 Wave type equation formulation

Eq.(1) is a wave type equation. This can be seen more easily if certain external forces are considered to be zero, $\mathbf{f}(t, s) = \mathbf{0}$, and the tension is treated as constant, $T(t, s) = T$. These considerations, although not being true in general, are useful to relate the mooring line dynamics with a wave type equation.

Under these conditions, Eq.(1) transforms into the following:

$$\gamma_0 \frac{\partial^2 \mathbf{r}(t, s)}{\partial t^2} = T \frac{\partial^2 \mathbf{r}(t, s)}{\partial s^2}$$

which allows to express Eq.(3) and the whole problem as a wave equation:

$$\left\{ \begin{array}{ll} \frac{\partial^2 \mathbf{r}(t, s)}{\partial t^2} = v^2 \frac{\partial^2 \mathbf{r}(t, s)}{\partial s^2} & \text{if } s \in (0, L), t > 0 \\ \mathbf{r}(t, 0) = \mathbf{r}_0 & \text{if } t > 0 \\ \mathbf{r}(t, L) = \mathbf{r}_F(t) & \text{if } t > 0 \\ \mathbf{r}(0, s) = \mathbf{g}(s) & \text{if } s \in (0, L) \\ \frac{\partial \mathbf{r}(0, s)}{\partial t} = \mathbf{0} & \text{if } s \in (0, L) \end{array} \right. \begin{array}{l} \text{PDE system} \\ \text{Boundary conditions} \\ \text{Initial conditions} \end{array}$$

being $v = \sqrt{\frac{T}{\gamma_0}}$ the wave velocity, with units of m/s .

2.3 Brief description a more complex model

This work is based on the model described in subsection 2.1, which is a simplification of a more complex model of the mooring line dynamics described by Rodríguez et al. (2020) based on the following non-linear equation:

$$\gamma_0 \frac{\partial^2 \mathbf{r}(t, s)}{\partial t^2} = \frac{\partial}{\partial s} \left(T(t, s) \frac{\frac{\partial \mathbf{r}(t, s)}{\partial s}}{\left| \frac{\partial \mathbf{r}(t, s)}{\partial s} \right|} \right) + \mathbf{f}(t, s)(1 + e(t, s)) \quad (4)$$

where $e : [0, \infty) \times [0, L] \rightarrow \mathbb{R}$ is the strain, defined by:

$$\left| \frac{\partial \mathbf{r}(t, s)}{\partial s} \right| = 1 + e(t, s).$$

In general, $e(t, s)$ is a small quantity, almost infinitesimal. In the model used in this work, the strain is considered to be zero, $e(t, s) = 0$, leading to $\left| \frac{\partial \mathbf{r}(t, s)}{\partial s} \right| = 1$, which corresponds to the theoretical definition of the arc length variable s . This approximation allows to reduce the above expression Eq.(4) to the previously introduced Eq.(1).

Considering the strain introduces a non-linearity and greatly complicates the development of the numerical method developed in section 4. The description of the numerical method with this dynamic model is outside the scope of this work, although the mooring line dynamics were modelled with this behaviour in Desiré et al. (2022).

Therefore, the general expression formulated in Eq.(3) can be described in this particular case as

$$\left\{ \begin{array}{ll} \frac{d}{ds} \left(T(s) \frac{d\mathbf{r}(s)}{ds} \right) + \mathbf{f}(s) = 0 & \text{if } s \in (0, L) \quad \text{ODE system} \\ \mathbf{r}(0) = \mathbf{r}_0 & \text{if } s = 0 \\ \mathbf{r}(L) = \mathbf{r}_F & \text{if } s = L \quad \text{Boundary conditions} \end{array} \right. \quad (5)$$

where the PDE system has been transformed into a ODE system because the whole formulation depends on a single variable s and the initial condition of the position is trivial $\mathbf{r}(s) = \mathbf{g}(s)$.

An analytic expression can describe the behaviour of a mooring line subject to the previous exposed conditions. The next section 3.2 describes the process developed until the solution of Eq.(3) under these circumstances was found.

3.2 Analytical resolution

The objective of this section is to find an analytical expression for a static mooring line subject to an horizontal known force H in the previous introduced conditions.

In order to parameterize this problem, the mooring can be divided in two parts: one laying in the slope until a certain point \mathbf{P}_1 , and the other part, which forms a catenary. Therefore, the followed steps in order to obtain the analytical solution are the following:

- 1^o Deduction of the catenary equation
- 2^o Parameterization of the catenary part of the mooring, which goes from \mathbf{P}_1 to the fairlead position, \mathbf{r}_F .
- 3^o Parameterization of the part of the mooring following the seabed surface, which goes from the anchor position, \mathbf{r}_0 to \mathbf{P}_1 .
- 4^o Determination of l_0 , the length of the mooring line until the point \mathbf{P}_1 .
- 5^o Combination of the last two steps in order to describe a total and continuous parameterization which depends on a single arc-length variable, s .

3.2.1 Deduction of catenary equation

The first step to obtain a parameterization of the catenary part of the mooring, is to develop the corresponding equation, which has been performed following Simmons (1985)'s method. The elected system of reference in this deduction has the origin in the catenary apex.

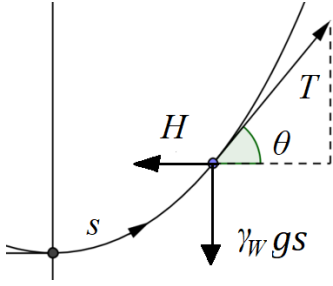


Figure 3: Catenary tension T produced by an horizontal force H and the weight of the catenary ($\gamma_W g s$).

Let a mooring submerged into the water form a catenary. By the Figure 3, it can be seen that

$$\begin{aligned} H &= T \cos \theta \\ \gamma_W g s &= T \sin \theta \end{aligned} \quad (6)$$

where γ_W is the mooring line mass per unit of length inside the water, $g = 9.8 m/s^2$ is the gravity acceleration and s is the arc length parameter of the catenary. T is the mooring line total tension, θ is the tension angle, and H is the horizontal applied force. The effective weight of the mooring inside the water is $\gamma_W g s$.

The characteristic length of the catenary, λ , is defined as follows:

$$\lambda = \frac{H}{\gamma_W g}. \quad (7)$$

By dividing both terms in Eq.(6) and using the definition of λ in Eq.(7), the following expression is obtained:

$$\frac{s}{\lambda} = \tan \theta = \frac{dy}{dx} \quad (8)$$

and deriving by x variable:

$$\frac{1}{\lambda} \frac{ds}{dx} = \frac{d^2 y}{dx^2}.$$

Using the definition of the derivative of arc-length that comes from Pythagorean theorem ($ds^2 = dx^2 + dy^2$), $\frac{ds}{dx} = \sqrt{1 + \left(\frac{dy}{dx}\right)^2}$ and creating a new variable $q = \frac{dy}{dx}$, the previous expression is reduced to:

$$\frac{1}{\lambda} \sqrt{1 + q^2} = \frac{dq}{dx}.$$

Integrating both terms

$$\int \frac{dx}{\lambda} = \int \frac{dq}{\sqrt{1 + q^2}}$$

one of the possible solutions to the integrals above is:

$$\ln(\sqrt{1 + q^2} + q) = \frac{x}{\lambda}.$$

Leading to the following expressions:

$$\begin{aligned} e^{x/\lambda} &= \sqrt{1 + q^2} + q \\ e^{-x/\lambda} &= \frac{1}{\sqrt{1 + q^2} + q} = \sqrt{1 + q^2} - q \end{aligned}$$

which allow to express q as:

$$\frac{dy}{dx} = q = \frac{e^{x/\lambda} - e^{-x/\lambda}}{2}$$

whose general solution is the following

$$y = \lambda \frac{e^{x/\lambda} + e^{-x/\lambda}}{2} + c_4,$$

where c_4 is a variable constant. It can be seen that when $x = 0$, $y = \lambda + c_4$. Therefore, in order to define the apex at $(0,0)$, $c_4 = -\lambda$. Finally, the catenary equation for a system of reference with its origin in the catenary apex is obtained:

$$y = \lambda \left(\cosh \left(\frac{x}{\lambda} \right) - 1 \right) \quad (9)$$

3.2.2 Parameterization of the catenary part

It must be remarked that the procedure followed in this section is based on the one used by Batista and Perkovic (2019).

The catenary part goes from the point P_1 to the fairlead position, \mathbf{r}_F . As l_0 is the length of the part of the mooring laying on the slope, the length of the catenary part will be $L - l_0$. Arc-length variable s is a convenient notation for these type of problems, which is defined as follows:

$$s = \lambda \sinh \left(\frac{x}{\lambda} \right) \text{ with } s \in [s_1, L - l_0 + s_1]$$

being s_1 the arc-length point which determines the start of the parameterization or in other words, the arc-length corresponding to the point \mathbf{P}_1 . In order to determine s_1 , it should be remembered that \mathbf{P}_1 has an inclination of $-\alpha$. If Eq.(8) is applied, it leads to

$$s_1 = -\lambda \tan(\alpha). \quad (10)$$

The definition of the arc-length parameter s provides a relation between X-coordinate and s . By using that $\cosh^2(x) - \sinh^2(x) = 1$, it is obtained that

$$\cosh \left(\frac{x}{\lambda} \right) = \sqrt{1 + \left(\frac{s}{\lambda} \right)^2}.$$

Substituting this value in the catenary equation provided in Eq.(9) leads to the following expression:

$$\begin{aligned} x &= \lambda \cdot \operatorname{asinh} \left(\frac{s}{\lambda} \right) \\ y &= \lambda \left(\sqrt{1 + \left(\frac{s}{\lambda} \right)^2} - 1 \right) \end{aligned} \quad (11)$$

which is the catenary description parameterized by its arc length coordinate s in a coordinate system where the origin is the apex.

However, as it has been previously described, in the presented work the coordinate system has its origin at the fairlead position \mathbf{r}_F . In that frame, the apex coordinates can be expressed as (X_0, Y_0) , and the previous expression transforms into the following:

$$\begin{aligned} X &= X_0 + \lambda \cdot \operatorname{asinh} \left(\frac{s}{\lambda} \right) \\ Y &= Y_0 + \lambda \left(\sqrt{1 + \left(\frac{s}{\lambda} \right)^2} - 1 \right) \end{aligned}$$

Nevertheless, the apex coordinates (X_0, Y_0) are unknown whereas $\mathbf{P}_1 = (X_1, Y_1)$ will be determined by Eq.(15), as it will be further discussed. Therefore, the following expression can be used to express (X_0, Y_0) in terms of \mathbf{P}_1 :

$$\begin{aligned} X_0 &= X_1 - \lambda \cdot \operatorname{asinh}\left(\frac{s_1}{\lambda}\right) &= X_1 + \lambda \cdot \operatorname{asinh}(\tan(\alpha)) \\ Y_0 &= Y_1 - \lambda \left(\sqrt{1 + \left(\frac{s_1}{\lambda}\right)^2} - 1 \right) &= Y_1 - \lambda \left(\sqrt{1 + \tan^2(\alpha)} - 1 \right) \end{aligned}$$

where the definition of s_1 provided by Eq.(10) has been used.

Finally, by joining the last two expressions, it is obtained the final parameterization of the catenary in terms of its arc-length coordinate s :

$$\mathbf{r}_{\text{cat}}(s) = \begin{cases} r_{\text{cat}, X}(s) &= X_1 + \lambda \cdot \operatorname{asinh}\left(\frac{s}{\lambda}\right) + \lambda \cdot \operatorname{asinh}(\tan(\alpha)) \\ r_{\text{cat}, Y}(s) &= Y_1 + \lambda \left(\sqrt{1 + \left(\frac{s}{\lambda}\right)^2} - \sqrt{1 + \tan^2(\alpha)} \right) \end{cases} \quad (12)$$

with $s \in [-\lambda \tan(\alpha), L - l_0 - \lambda \tan(\alpha)]$

To complete this expression, $\mathbf{P}_1 = (X_1, Y_1)$ coordinates must be determined, which can be done by applying Eq.(15) below.

It is interesting to get the analytical expression for the tension of the catenary points, specifically at the fairlead \mathbf{r}_F , which is a easily measurable quantity used in a lot of experimental tests that can verify the correct behaviour of the proposed analytical solution. Regarding Eq.(6), the total tension T at a catenary point with arc-length parameter s can be obtained the following way:

$$T(s) = \sqrt{H^2 + (\gamma_W g s)^2} = H \sqrt{1 + \left(\frac{s}{\lambda}\right)^2} \quad \text{with } s \in [-\lambda \tan(\alpha), L - l_0 - \lambda \tan(\alpha)] \quad (13)$$

where the introduced definition of λ in Eq.(7) has been used. The tension at the fairlead can be easily calculated by replacing s by $L - l_0 - \lambda \tan(\alpha)$, as it will be done in the results (see section 5).

3.2.3 Parameterization of the part which lays on the slope

From the anchor $\mathbf{r}_0 = (r_{0,x}, r_{0,y})$ to the point \mathbf{P}_1 , the mooring line follows the seabed surface. Let l_0 be the length of this part of the line. Then, the mooring can be parametrized as:

$$\mathbf{r}_{\text{slope}}(s) = \begin{cases} r_{\text{slope}, X}(s) &= r_{0,x} + s \cdot \cos(\alpha) \\ r_{\text{slope}, Y}(s) &= r_{0,y} - s \cdot \sin(\alpha) \end{cases} \quad \text{with } s \in [0, l_0] \quad (14)$$

where s is the arc parameter of this part of the mooring. l_0 is determined by Eq.(16) developed in the next section. Once l_0 is obtained, by substituting s by l_0 in the parameterization of the slope part described in Eq.(14), \mathbf{P}_1 coordinates can be obtained:

$$\mathbf{P}_1 = (r_{0,x} + l_0 \cdot \cos(\alpha), r_{0,y} - l_0 \cdot \sin(\alpha)). \quad (15)$$

3.2.4 Determination of l_0

Calculating l_0 allows to determine \mathbf{P}_1 coordinates with Eq.(15) as well as the arc-length parameters defined in Eq.(12), completing the expression.

However, as \mathbf{P}_1 is not determined yet, in this deduction, the catenary apex has been considered as the frame origin. Then, \mathbf{r}_F is not located at (0,0) in this section. This will not affect the calculation of l_0 distance.

By Figure 2 the following relation can be induced:

$$\Delta y = r_{F,y} - Y_1 = l_0 \sin(\alpha) + h_A$$

where h_A is the distance from the anchor to the sea level, in other words, $h_A = -r_{0,y}$. As the current frame is the one that has the origin in the catenary apex, the catenary equation described for this frame of reference in Eq.(11) can be used:

$$\lambda \left[\sqrt{1 + \left(\frac{s_2}{\lambda}\right)^2} - 1 \right] - \lambda \left[\sqrt{1 + \left(\frac{s_1}{\lambda}\right)^2} - 1 \right] = l_0 \sin(\alpha) + h_A$$

where s_1 and s_2 are the catenary arc-length parameters of the points P_1 and \mathbf{r}_F respectively. It should be remembered that the length of this mooring line part is $L - l_0$, leading to $s_2 = L - l_0 + s_1$. Then, the definition of s_1 provided in Eq.(10) is applied:

$$\sqrt{\lambda^2 + (L - l_0 - \lambda \tan(\alpha))^2} - \sqrt{\lambda^2 + \lambda^2 \tan^2(\alpha)} = l_0 \sin(\alpha) + h_A.$$

In addition, the variable p was created:

$$p = \tan(\alpha) \Rightarrow \sin(\alpha) = \frac{\sin(\alpha)}{\sqrt{\sin^2(\alpha) + \cos^2(\alpha)}} = \frac{\tan(\alpha)}{\sqrt{1 + \frac{\sin^2(\alpha)}{\cos^2(\alpha)}}} = \frac{p}{\sqrt{1 + p^2}}.$$

Substituting p into the previous equation, the following expression is obtained:

$$\sqrt{\lambda^2 + (L - l_0 - \lambda p)^2} - \lambda \sqrt{1 + p^2} = h_A + l_0 \frac{p}{\sqrt{1 + p^2}}.$$

After doing some calculations, the following quadratic equation is obtained:

$$l_0^2 - 2l_0 \left[L(1 + p^2) + h_A p \sqrt{1 + p^2} \right] + (1 + p^2) \left[L - 2L\lambda p - h_A^2 - 2\lambda h_A \sqrt{1 + p^2} \right] = 0$$

providing a unique realistic solution that has been taken from Batista and Perkovic (2019):

$$l_0 = L(1 + p^2) + \sqrt{1 + p^2} \left[h_A p - \sqrt{h_A^2 + 2h_A(\lambda + Lp)\sqrt{1 + p^2} + 2\lambda Lp + (L^2 + h_A^2)p^2} \right] \quad (16)$$

3.2.5 Final solution

Both of the mooring line parts (the catenary and the slope) separated by \mathbf{P}_1 can be joined in a common expression $\mathbf{r}(s)$ with $s \in [0, L]$ that is the solution of the proposed problem in Eq.(5).

The parameterization corresponding to the part of the mooring line laying on the slope described by Eq.(14) goes from the anchor \mathbf{r}_0 , which corresponds to $s = 0$, to the point \mathbf{P}_1 , corresponding to $s = l_0$.

Then, the part of the mooring line which described a catenary shown in Eq.(12) was defined with $s \in [-\lambda \tan(\alpha), L - l_0 - \lambda \tan(\alpha)]$ whereas in the desired general description, the arc-length parameter in this part should be described by $s \in [l_0, L]$. This is achieved by a simple translation of the arc-parameter.

$$\mathbf{r}_{\text{cat}}(s - l_0 - \lambda \tan(\alpha)) = \mathbf{r}(s)$$

which verifies the desired condition: $\mathbf{r}(l_0) = \mathbf{r}_{\text{cat}}(-\lambda \tan(\alpha)) = \mathbf{P}_1$ and $\mathbf{r}(L) = \mathbf{r}_{\text{cat}}(L - l_0 - \lambda \tan(\alpha)) = \mathbf{r}_F$. Then, the following continuous solution is obtained:

$$\mathbf{r}(s) = \begin{cases} \mathbf{r}_{\text{slope}}(s) & \text{if } s \in [0, l_0] \\ \mathbf{r}_{\text{cat}}(s - l_0 - \lambda \tan(\alpha)) & \text{if } s \in (l_0, L] \end{cases} \quad (17)$$

With this expression, it is possible to reproduce analytically the behaviour of the complete mooring in the described situation. Later, in subsection 5.1, the results provided by this equation will be compared with the ones obtained numerically by the method developed in section 4, showing great accordance.

3.2.6 Verification of the obtained expressions

The obtained solution $\mathbf{r}(s)$ must verify the formulation of the considered problem described in Eq.(5). Therefore, both parts of the mooring line, $\mathbf{r}_{\text{cat}}(s)$ and $\mathbf{r}_{\text{slope}}(s)$, must accomplish the ODE system. On the other hand, the boundary conditions are accomplished by the proper definition of the expressions, which have been constructed with this propose.

- Checking that $\mathbf{r}_{\text{cat}}(s)$ verifies the ODE system:

$\mathbf{r}_{\text{cat}}(s)$, which was described in Eq.(12) satisfies:

$$\begin{aligned} \frac{d}{ds} \mathbf{r}_{\text{cat}, X} &= \lambda \frac{1/\lambda}{\sqrt{1 + (\frac{s}{\lambda})^2}} = \lambda / \sqrt{\lambda^2 + s^2} \\ \frac{d}{ds} \mathbf{r}_{\text{cat}, Y} &= \lambda \frac{2s/\lambda^2}{2\sqrt{1 + (\frac{s}{\lambda})^2}} = s / \sqrt{\lambda^2 + s^2} \end{aligned}$$

verifying $(\frac{d}{ds} \mathbf{r}_{\text{cat}, X})^2 + (\frac{d}{ds} \mathbf{r}_{\text{cat}, Y})^2 = \frac{\lambda^2}{\lambda^2 + s^2} + \frac{s^2}{\lambda^2 + s^2} = 1$, which is the arc-length definition.

If the tension expression formulated in Eq.(13) and the definition of λ provided in Eq.(7) are used:

$$T(s) = \sqrt{(\gamma_W g s)^2 + H^2} = \gamma_W g \sqrt{\lambda^2 + s^2}$$

obtaining:

$$\begin{aligned}\frac{d}{ds} \left(T(s) \frac{d}{ds} \mathbf{r}_{\text{cat},X} \right) &= \frac{d}{ds} \lambda \gamma_W g = 0 \\ \frac{d}{ds} \left(T(s) \frac{d}{ds} \mathbf{r}_{\text{cat},Y} \right) &= \frac{d}{ds} \gamma_W g s = \gamma_W g\end{aligned}$$

whereas the only external force per unit of length that appears from the ones considered in Eq.(2) is the effective weight per unit of length, $\mathbf{f}_{bg}(s) = -\gamma_W g$, which is in the Y-axis:

$$\mathbf{f}(s) = (0, -\gamma_W g),$$

satisfying the ODE system which describes the mooring dynamics.

$$\frac{d}{ds} \left(T(s) \frac{d\mathbf{r}_{\text{cat}}(s)}{ds} \right) + \mathbf{f}(s) = (0, 0)$$

- Checking that the part of the mooring which lays on the slope $\mathbf{r}_{\text{slope}}(s)$ verifies the ODE system:

Based on the parameterization of $\mathbf{r}_{\text{slope}}$ shown in Eq.(14):

$$\begin{aligned}\frac{d}{ds} \mathbf{r}_{\text{slope}, X} &= \cos(\alpha) \\ \frac{d}{ds} \mathbf{r}_{\text{slope}, Y} &= -\sin(\alpha)\end{aligned}$$

which do also verify the arc length definition, $\left(\frac{d}{ds} \mathbf{r}_{\text{slope}, X} \right)^2 + \left(\frac{d}{ds} \mathbf{r}_{\text{slope}, Y} \right)^2 = 1$.

This time, the tension is constant ($T(s) = T$) because the angle of inclination is fixed (α). Therefore,

$$\frac{d}{ds} \left(T \frac{d\mathbf{r}_{\text{slope}}(s)}{ds} \right) = (0, 0)$$

whereas the external forces that intervene in this process from the ones considered in Eq.(2) are again the effective weight per unit of length $\mathbf{f}_{bg}(s)$ and the ones which appear when the mooring touches the seabed: the normal $\mathbf{f}_n(s)$ and friction $\mathbf{f}_f(s)$ forces per unit of length. However, by definition, in a static system, all these forces sum zero, as it can be seen in Figure 4. This leads to $\mathbf{f}(s) = (0, 0)$, which satisfies the ODE system

$$\frac{d}{ds} \left(T(s) \frac{d\mathbf{r}_{\text{slope}}(s)}{ds} \right) + \mathbf{f}(s) = (0, 0)$$

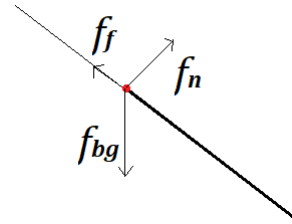


Figure 4: Forces in the part of the mooring which lays on the slope. $\mathbf{f}_{bg}(s)$ is the effective weight, $\mathbf{f}_n(s)$ is the normal force and $\mathbf{f}_f(s)$ the friction force.

4 Three dimensional general case

In this section, the mooring is described into its three dimensions. Its fairlead is free to move, which makes the mooring line vary its position along the time. Therefore, there is no static approach able to simplify the general problem formulation described in Eq.(3). A numerical method must be developed, which will be described in subsection 4.1. The necessary initial condition to describe the mooring dynamics is obtained by searching the static equilibrium in the mooring line, as it will be discussed in subsection 4.3.

In the subsection 4.2, a continuous projection algorithm has been constructed and integrated in the general previous existing numerical method developed by *IHCantabria* Rodríguez et al. (2020), allowing the mooring simulation to interpret an irregular seabed surface.

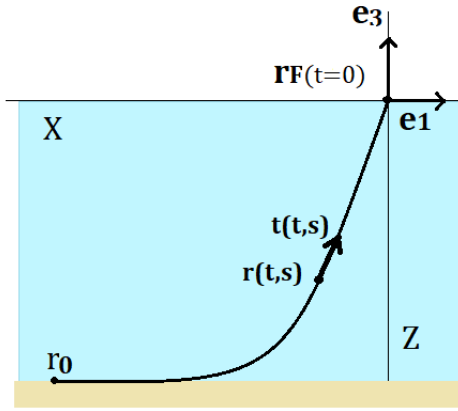


Figure 5: Coordinate system used. A view of the plane XZ can be seen.

The three dimensional used frame can be seen in Figure 5. The defined Y axis in the previous section 3 becomes now the Z axis, reaching $Z = 0$ at the sea surface and with e_3 pointing over the sea level, giving negative Z-values for the mooring depth. The newly defined Y axis describes the width of the mooring line and X axis keeps parallel to the length of the mooring, as it is described in the left image. The origin is the fairlead initial position, $\mathbf{r}_F(0)$.

4.1 Numerical method (FEM)

The objective is to solve numerically the problem formulated in Eq.(3), which is shown again:

$$\begin{cases}
 \gamma_0 \frac{\partial^2 \mathbf{r}(t,s)}{\partial t^2} = \frac{\partial}{\partial s} \left(T(t,s) \frac{\partial \mathbf{r}(t,s)}{\partial s} \right) + \mathbf{f}(t,s) & \text{if } s \in (0, L), t > 0 & \text{PDE system} \\
 \mathbf{r}(t, 0) = \mathbf{r}_0 & \text{if } t > 0 & \text{Boundary conditions} \\
 \mathbf{r}(t, L) = \mathbf{r}_F(t) & \text{if } t > 0 & \text{Boundary conditions} \\
 \mathbf{r}(0, s) = \mathbf{g}(s) & \text{if } s \in (0, L) & \text{Initial conditions} \\
 \frac{\partial \mathbf{r}(0,s)}{\partial t} = \mathbf{0} & \text{if } s \in (0, L) & \text{Initial conditions}
 \end{cases}$$

As it was previously discussed, the proposed problem can be understood as a wave type equation with a second order partial differential equation system (PDE System), two boundary conditions defined for the mooring line extremes ($\mathbf{r}(t, 0)$ and $\mathbf{r}(t, L)$) and two initial conditions that come from the order of the PDE system: initial positions ($\mathbf{r}(0, s)$) and the considered zero initial velocities ($\frac{\partial \mathbf{r}}{\partial t}(0, s)$). The remaining initial condition is defined by the function $\mathbf{g}(s)$, which will be calculated in subsection 4.3 and will be treated as known for the time being.

The numerical method used to solve the proposed problem is the finite element method (FEM). As a resume, FEM allows to transform the PDE system into a second order system of ordinary differential equations (ODEs) by discretizing the mooring line into N nodes and defining a basis of functions which allow to express the solution as a linear combination of them. The system can be solved numerically, providing the accelerations of the line nodes of the mooring line.

Finally, the second order ODE system can be reduced to first order, which allows to integrate and construct the temporal simulation.

4.1.1 Homogenization of the problem

As it will be further discussed, applying FEM is much more simple when the boundary conditions are null in the extremes, which is known as an homogeneous problem. This can be reached by constructing the following term $\hat{\mathbf{r}}(t, s)$:

$$\hat{\mathbf{r}}(t, s) = \frac{s}{L} \mathbf{r}_{\mathbf{F}}(t) + \left(1 - \frac{s}{L}\right) \mathbf{r}_0$$

and performing a change of unknown functions:

$$\tilde{\mathbf{r}}(t, s) = \mathbf{r}(t, s) - \hat{\mathbf{r}}(t, s).$$

The formulation of the problem described in Eq.(3) can be applied to $\tilde{\mathbf{r}}(t, s)$, obtaining the following expressions:

- PDE System

$$\begin{aligned} \gamma_0 \frac{\partial^2 \tilde{\mathbf{r}}(t, s)}{\partial t^2} - \frac{\partial}{\partial s} \left(T(t, s) \frac{\partial \tilde{\mathbf{r}}(t, s)}{\partial s} \right) &= \\ &= \gamma_0 \frac{\partial^2 \mathbf{r}(t, s)}{\partial t^2} - \frac{\partial}{\partial s} \left(T(t, s) \frac{\partial \mathbf{r}(t, s)}{\partial s} \right) - \gamma_0 \frac{\partial^2 \hat{\mathbf{r}}(t, s)}{\partial t^2} + \frac{\partial}{\partial s} \left(T(t, s) \frac{\partial \hat{\mathbf{r}}(t, s)}{\partial s} \right) = \\ &= \mathbf{f}(t, s) - \gamma_0 \frac{s}{L} \frac{d^2 \mathbf{r}_{\mathbf{F}}(t)}{dt^2} + \frac{\partial T(t, s)}{\partial s} \left(\frac{\mathbf{r}_{\mathbf{F}}(t)}{L} - \frac{\mathbf{r}_0}{L} \right) = \tilde{\mathbf{f}}(t, s). \end{aligned}$$

- Boundary conditions

$$\begin{aligned} \tilde{\mathbf{r}}(t, 0) &= \mathbf{r}(t, 0) - \mathbf{r}_0 = \mathbf{0} \\ \tilde{\mathbf{r}}(t, L) &= \mathbf{r}(t, L) - \mathbf{r}_{\mathbf{F}}(t) = \mathbf{0} \end{aligned}$$

- Initial conditions

$$\begin{aligned} \tilde{\mathbf{r}}(0, s) &= \mathbf{r}(0, s) - \frac{s}{L} \mathbf{r}_{\mathbf{F}}(0) - \left(1 - \frac{s}{L}\right) \mathbf{r}_0 = \tilde{\mathbf{g}}(s) \\ \frac{\partial \tilde{\mathbf{r}}(0, s)}{\partial t} &= \frac{\partial \mathbf{r}(0, s)}{\partial s} - \frac{s}{L} \frac{d \mathbf{r}_{\mathbf{F}}(0)}{dt} = -\frac{s}{L} \frac{d \mathbf{r}_{\mathbf{F}}(0)}{dt} \end{aligned}$$

As the boundary conditions are now null in the extremes, this change of unknown functions allows to express Eq.(3) as an homogeneous problem:

$$\begin{cases}
\gamma_0 \frac{\partial^2 \tilde{\mathbf{r}}(t,s)}{\partial t^2} = \frac{\partial}{\partial s} \left(T(t,s) \frac{\partial \tilde{\mathbf{r}}(t,s)}{\partial s} \right) + \tilde{\mathbf{f}}(t,s) & \text{if } s \in (0, L), t > 0 & \text{PDE system} \\
\tilde{\mathbf{r}}(t, 0) = \mathbf{0} & \text{if } t > 0 & \text{Boundary conditions} \\
\tilde{\mathbf{r}}(t, L) = \mathbf{0} & \text{if } t > 0 & \\
\tilde{\mathbf{r}}(0, s) = \tilde{\mathbf{g}}(s) & \text{if } s \in (0, L) & \text{Initial conditions} \\
\frac{\partial \tilde{\mathbf{r}}(0,s)}{\partial t} = -\frac{s}{L} \frac{d\mathbf{r}_F(0)}{dt} & \text{if } s \in (0, L) &
\end{cases} \tag{18}$$

Homogenizing the problem simplifies the next steps of the FEM method.

4.1.2 Weak formulation

FEM method is based on searching for the solution in a concrete space of functions, which is known as weak formulation. In order to understand the concept of weak formulation, Sobolev spaces must be introduced:

Definition 1 For a certain domain Ω and $m, p \in \mathbb{N}$, the Sobolev space of functions $W^{m,p}(\Omega)$ can be defined as:

$$W^{m,p}(\Omega) = \{f \in L^p(\Omega) \mid \partial^\alpha f \in L^p(\Omega) \forall |\alpha| \leq m\}$$

where ∂^α is the partial derivative of order α and $(L^p(\Omega), \|\cdot\|_p)$ is the normed function space.

The vector space $L^p(\Omega)$ is composed by the measurable functions $f : \Omega \rightarrow \mathbb{R}$ defined in the measurable space (Ω, μ) for which their integral satisfies $\int |f|^p d\mu < \infty$.

The p -norm which defines the normed function space is described as $\|\cdot\|_p = \sqrt[p]{\int |f|^p d\mu}$.

If, for a certain Sobolev space $p = 2$, the Sobolev space is dotted with Hilbert Space structure and can be expressed as:

$$H^m(\Omega) = \{f \in L^2(\Omega) \mid \partial^\alpha f \in L^2(\Omega) \forall |\alpha| \leq m\}$$

The unknown solution of the homogenized problem in Eq.(18) must satisfy the imposed boundary conditions, which are null in the mooring line extremes. Let V be an infinite dimension space composed of functions $w : \mathbb{R} \rightarrow \mathbb{R}$ which verify:

$$V = \{w(s) \in H^1([0, L]) \text{ that } w(0) = w(L) = 0\}$$

where $H^1([0, L]) = \{w(s) \in L^2([0, L]) \mid \frac{dw(s)}{ds} \in L^2([0, L])\}$ is the corresponding Sobolev space defined in the domain $[0, L]$ with $m = 1$, understanding derivatives in the sense of distributions.

It can be seen that, $\forall t, \tilde{\mathbf{r}}(t, s) \in V^3$ (with $V^3 = V \times V \times V$) which means that each of the coordinates of the solution is expected to be in the space V . Finite element method starts by

selecting a test function $w(s) \in V$. If the homogenized PDE system in Eq.(18 is multiplied by the test function $w(s)$, it is obtained:

$$\gamma_0 \frac{\partial^2 \tilde{\mathbf{r}}(t, s)}{\partial t^2} w(s) = \frac{\partial}{\partial s} \left(T(t, s) \frac{\partial \tilde{\mathbf{r}}(t, s)}{\partial s} \right) w(s) + \tilde{\mathbf{f}}(t, s) w(s).$$

Integrating along the length leads to the following expression

$$\int_0^L \gamma_0 \frac{\partial^2 \tilde{\mathbf{r}}(t, s)}{\partial t^2} w(s) ds = \int_0^L \frac{\partial}{\partial s} \left(T(t, s) \frac{\partial \tilde{\mathbf{r}}(t, s)}{\partial s} \right) w(s) ds + \int_0^L \tilde{\mathbf{f}}(t, s) w(s) ds$$

and integrating by parts

$$\int_0^L \gamma_0 \frac{\partial^2 \tilde{\mathbf{r}}(t, s)}{\partial t^2} w(s) ds = \left[T(t, s) \frac{\partial \tilde{\mathbf{r}}(t, s)}{\partial s} w(s) \right]_0^L - \int_0^L T(t, s) \frac{\partial \tilde{\mathbf{r}}(t, s)}{\partial s} \frac{d}{ds} w(s) ds + \int_0^L \tilde{\mathbf{f}}(t, s) w(s) ds.$$

Finally, using the properties of the test function $w(s) \in V$, $w(0) = w(L) = 0$, it is obtained:

$$\int_0^L \gamma_0 \frac{\partial^2 \tilde{\mathbf{r}}(t, s)}{\partial t^2} w(s) ds = - \int_0^L T(t, s) \frac{\partial \tilde{\mathbf{r}}(t, s)}{\partial s} \frac{d}{ds} w(s) ds + \int_0^L \tilde{\mathbf{f}}(t, s) w(s) ds \quad (19)$$

which is called the weak formulation of the problem, equivalent to finding the minimum error (minimization problem) in L^2 (Burden and Faires, 2013).

4.1.3 Discretization/ Galerkin continuous method

Finite element method lays on searching for the solution in a finite dimension subspace of the previously introduced V , which will be called V_N from now on.

The method starts by dividing the mooring line length into N equispaced nodes, $\{s_i\}_{i=0}^{N-1}$. V_N will have dimension N and its basis will be formed by the functions $\{\phi_i\}_{i=0}^{N-1} \in V$ which must satisfy $\phi_i(0) = \phi_i(L) = 0$ and will be later described in 4.1.4.

Once the basis is constructed, the mooring line position homogenized vector $\tilde{\mathbf{r}}(t, s)$ can be expressed as a linear combination of the basis elements:

$$\tilde{\mathbf{r}}(t, s) = \sum_{i=0}^{N-1} \mathbf{r}_i(t) \phi_i(s)$$

being $\mathbf{r}_i(t) = \tilde{\mathbf{r}}(s_i, t)$ the mooring line nodes positions: three-coordinate vectors which contain the position of each node i . On the other hand, $\phi_i(s)$ are scalar functions. The tangential vector, which is the spatial derivative of the mooring line position vector $\frac{\partial \tilde{\mathbf{r}}(t, s)}{\partial s}$ can be calculated as follows:

$$\frac{\partial \tilde{\mathbf{r}}(t, s)}{\partial s} = \sum_{i=0}^{N-1} \mathbf{r}_i(t) \frac{d\phi_i(s)}{ds}.$$

The discretization is also applied to external force vectors.

$$\mathbf{f}(t, s) = \sum_{i=0}^{N-1} \mathbf{f}_i(t) \phi_i(s).$$

The test function $w(s) \in V$ used in the weak formulation is chosen to be a function of the basis of V_N , $w(s) = \phi_j(s)$. If the described discretizations are applied to the integral in Eq.(19), it is obtained that:

$$\begin{aligned} \gamma_0 \int_0^L \left(\sum_{i=0}^{N-1} \frac{\partial^2 \mathbf{r}_i(t)}{\partial t^2} \phi_i(s) \right) \phi_j(s) ds &= \dots \\ \dots &= - \int_0^L \left(\sum_{i=0}^{N-1} T(t, s) \mathbf{r}_i(t) \frac{d\phi_i(s)}{ds} \right) \frac{d\phi_j(s)}{ds} ds + \int_0^L \left(\sum_{i=0}^{N-1} \mathbf{f}_i(t) \phi_i(s) \right) \phi_j(s) ds \end{aligned}$$

which can be expressed as

$$\gamma_0 \sum_{i=0}^{N-1} \frac{\partial^2 \mathbf{r}_i(t)}{\partial t^2} \int_0^L \phi_i(s) \phi_j(s) ds = - \sum_{i=0}^{N-1} \mathbf{r}_i(t) \int_0^L T(t, s) \frac{d\phi_i(s)}{ds} \frac{d\phi_j(s)}{ds} ds + \sum_{i=0}^{N-1} \mathbf{f}_i(t) \int_0^L \phi_i(s) \phi_j(s) ds,$$

obtaining a second order system of ODEs, as the equations depend only on time:

$$\gamma_0 M \begin{pmatrix} \frac{d^2 \mathbf{r}_0(t)}{dt^2} \\ \frac{d^2 \mathbf{r}_1(t)}{dt^2} \\ \vdots \\ \frac{d^2 \mathbf{r}_{N-1}(t)}{dt^2} \end{pmatrix} = -K(t) \begin{pmatrix} \mathbf{r}_0(t) \\ \mathbf{r}_1(t) \\ \vdots \\ \mathbf{r}_{N-1}(t) \end{pmatrix} + M \begin{pmatrix} \mathbf{f}_0(t) \\ \mathbf{f}_1(t) \\ \vdots \\ \mathbf{f}_{N-1}(t) \end{pmatrix} \quad (20)$$

being

$$M_{i,j} = \int_0^L \phi_i(s) \phi_j(s) ds$$

and

$$K_{i,j}(t) = \int_0^L T(t, s) \frac{d\phi_i(s)}{ds} \frac{d\phi_j(s)}{ds} ds.$$

In FEM method, M is commonly referred as mass matrix while $K(t)$ is the stiffness matrix.

4.1.4 Definition of the basis

The election of the basis functions $\{\phi_i\}_{i=0}^{N-1}$ is specially important in order to reduce the computational cost in solving the system in Eq.(20). This is achieved by constructing sparse matrices, which starts by defining linear basis functions:

$$\phi_i(s) = \begin{cases} 0 & \text{if } s < s_{i-1} \\ (s - s_{i-1})/l & \text{if } s_{i-1} \leq s < s_i \\ (-s + s_{i+1})/l & \text{if } s_i \leq s < s_{i+1} \\ 0 & \text{if } s_{i+1} \leq s \end{cases}$$

where $l = L/(N - 1)$ is the length of an interval and $\{s_i\}_{i=0}^{N-1}$ are the mooring line nodes. These basis functions have been chosen following the steps in Aamo and Fossen (2000). The advantage provided by these functions is that they accomplish the following condition:

$$\int_0^L \phi_i(s) \phi_j(s) ds = 0 \quad \forall j \neq \{i, i - 1, i + 1\}.$$

Then, the matrix M in the ODE system in Eq.(20) becomes tridiagonal.

It is also interesting to study the derivatives of the basis functions, which are defined as follows:

$$\frac{d\phi_i(s)}{ds} = \begin{cases} 0 & \text{if } s < s_{i-1} \\ 1/l & \text{if } s_{i-1} \leq s < s_i \\ -1/l & \text{if } s_i \leq s < s_{i+1} \\ 0 & \text{if } s_{i+1} \leq s \end{cases}$$

It can be seen that the derivatives are well defined in the Sobolev space H^1 , because as it has been said, they must be understood in the sense of distributions. Again,

$$\frac{d\phi_i(s)}{ds} \frac{d\phi_j(s)}{ds} = 0 \quad \forall j \neq \{i, i-1, i+1\},$$

making the stiffness matrix $K(t)$ in the ODE system in Eq.(20) tridiagonal.

The functions $\phi_i(s)$ may be easier to understand with this Figure:

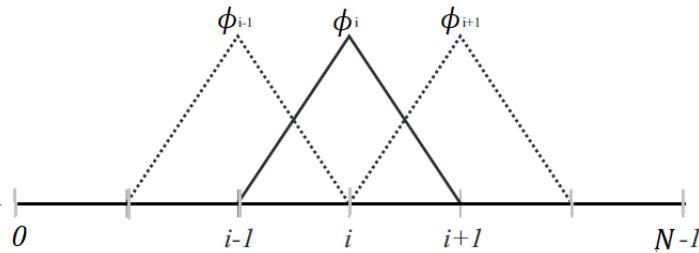


Figure 6: Representation of the basis functions used in the developed finite element method. The image has been taken from Aamo and Fossen (2000).

The election of the functions which construct the basis is not unique: there are other approaches which use higher order functions as a basis, for example B-splines or higher order polynomials (Burden and Faires, 2013). The advantage of these approaches is that they provide a continuous derivative without needing to define it in the sense of distributions. However, using these other functions introduces more terms in the mass and stiffness matrices, producing an increment in the computational cost of solving the ODE system in Eq.(20) as long as the number of mooring line nodes is not decreased.

4.1.5 From second order to first order ODEs system

The final expression obtained by FEM, which was Eq.(20), was a second order system of ODEs which did only depend on time. However, there is a general procedure which allows to reduce the order of the ODEs by duplicating the number of equations defining the system.

From Eq.(20) it is obtained that

$$\frac{d^2 \mathbf{r}_i(t)}{dt^2} = -\frac{1}{\gamma_0} M^{-1} K(t) \mathbf{r}_i(t) + \frac{1}{\gamma_0} \mathbf{f}_i(t) \quad \forall i \in \{0, \dots, N-1\}$$

Let $\mathbf{u}_i(t) = \mathbf{r}_i(t)$ and $\mathbf{v}_i(t) = \frac{d\mathbf{r}_i(t)}{dt} \forall i \in \{0, \dots, N-1\}$. It is obtained that

$$\frac{d\mathbf{u}_i(t)}{dt} = \mathbf{v}_i(t); \quad \frac{d\mathbf{v}_i(t)}{dt} = \frac{d^2\mathbf{r}_i(t)}{dt^2} = -\frac{1}{\gamma_0}M^{-1}K(t)\mathbf{u}_i(t) + \frac{1}{\gamma_0}\mathbf{f}_i(t) \quad \forall i \in \{0, \dots, N-1\}$$

which can be reordered in a linear system that must be solved $\forall i \in \{0, \dots, N-1\}$:

$$\begin{pmatrix} \frac{d\mathbf{u}_i(t)}{dt} \\ \frac{d\mathbf{v}_i(t)}{dt} \end{pmatrix} = \begin{pmatrix} 0 & 1 \\ -\frac{1}{\gamma_0}M^{-1}K(t) & 0 \end{pmatrix} \begin{pmatrix} \mathbf{u}_i(t) \\ \mathbf{v}_i(t) \end{pmatrix} + \begin{pmatrix} 0 \\ \frac{1}{\gamma_0}\mathbf{f}_i(t) \end{pmatrix}$$

4.2 Continuous projection algorithm

The mooring line is subject to several external forces, which were introduced in Eq.(2). Two of these forces depend on the seafloor structure: ground normal and friction forces. In order to reproduce them with accuracy, the interaction between the mooring line and the seafloor should be evaluated.

If these two forces are ignored, the external vector force in Eq.(1) will not be complete, and the numerical solution found by the finite element method may not be appropriate. This way, the objective is to calculate the terms of these two forces which are able to quantify the mooring line and seafloor, for whatever the seabed surface is.

4.2.1 Definition of the terms

Let S be the seabed surface. As it was defined above, $\{\mathbf{r}_i\}_{i \in 0, \dots, N-1}$ is the position of a mooring line node i and it is a three dimensional vector with the point coordinates.

For a particular mooring line node \mathbf{r}_i , let \mathbf{r}'_i be the closest point to \mathbf{r}_i contained in the surface S . In other words, it is the point which satisfies the following condition:

$$\mathbf{r}'_i \in S \mid \forall \mathbf{r}_G \in S, \|\mathbf{r}_i - \mathbf{r}'_i\| \leq \|\mathbf{r}_i - \mathbf{r}_G\|.$$

\mathbf{r}'_i is the projection of the mooring line node \mathbf{r}_i in the surface. For non-convex surfaces, the projection point may not be unique, but this problem has already been considered in 4.2.3.

In the projection point \mathbf{r}'_i , the unitary normal vector to the seabed surface S pointing outwards the sea (in the positive direction of Z axis) is defined as $\mathbf{n}_{S,i}$. With this definition, it is possible to introduce the terms needed to describe friction and ground forces:

- $\mathbf{d}_{P,i}$ is the direction of projection, a unitary vector pointing to the sea level described by:

$$\mathbf{d}_{P,i} = \mathbf{n}_{S,i} \tag{21}$$

- $d_{G,i}$ is the penetration depth of the mooring line node i in the seabed S , a scalar quantity defined as follows:

$$d_{G,i} = (\mathbf{r}_i - \mathbf{r}'_i) \cdot \mathbf{n}_{S,i} \tag{22}$$

$d_{G,i}$ is positive when the mooring line is over the seabed surface (when the vector $\overrightarrow{\mathbf{r}'_i\mathbf{r}_i}$ points to the sea level) and negative when it is buried into it.

Figure 7 describes graphically the introduced terms:

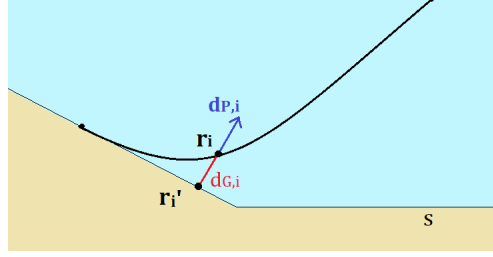


Figure 7: Graphical description of the terms $d_{G,i}$ (in red, a scalar) and $\mathbf{d}_{P,i}$ (in blue, a vector) for a certain mooring line (blue) node i in a surface S (black). \mathbf{r}_i is the vector position of the mooring line node and \mathbf{r}'_i its projection position.

These terms are obtained by a continuous projection method described in the following sections. The proposed projection method is suitable to be applied at any type of seafloor. However, if the seafloor surface is an inclined or horizontal plane, (which are commonly found structures) the general method can be replaced by a point-to-plane projection expression, reducing the computational cost required in these cases.

4.2.2 Specific cases: Horizontal or inclined plane seabed surface

In this subsection, the projection process for both horizontal or inclined plane seabeds is described. Figure 8 schemes the proposed method. Let \mathbf{r}_i be the position vector of a mooring line node i and \mathbf{r}'_i be the position vector of the projected line node i .

The case in which the floor is an horizontal plane, which is the used seafloor surface description in most of mooring simulations, is the simplest one. The projected point \mathbf{r}'_i has the same X and Y coordinates as the mooring line node \mathbf{r}_i ($r_{i,x} = r'_{i,x}$ and $r_{i,y} = r'_{i,y}$), while its z-coordinate is the same as the seafloor height, z_g ($r'_{i,z} = z_g$). The direction of projection always follows the Z axis, $\mathbf{d}_{P,i} = \mathbf{e}_3$.

Therefore, when the seafloor defines an horizontal plane, the previously introduced terms $d_{G,i}$ defined in Eq.(22) and $\mathbf{d}_{P,i}$ in Eq.(21) are the following:

$$\text{Horizontal plane} \begin{cases} \mathbf{d}_{P,i} = \mathbf{e}_3 \\ d_{G,i} = r_{i,z} - z_g. \end{cases} \quad \forall i \in \{0, \dots, N-1\}$$

On the other hand, when the seabed structure forms an inclined plane, its unitary normal vector pointing upwards \mathbf{n} defines the direction of projection for every mooring line node, $\mathbf{d}_{P,i} = \mathbf{n}$.

To obtain the projected mooring line nodes coordinates \mathbf{r}'_i , it must be noticed that \mathbf{r}'_i is contained in the inclined plane which defines the seabed surface and satisfies its equation:

$$\mathbf{r}'_i \cdot \mathbf{n} = k.$$

In addition, \mathbf{r}'_i is contained in the line with direction \mathbf{n} that also contains \mathbf{r}_i . Therefore, it satisfies the following parametric equation:

$$\mathbf{r}'_i = \mathbf{r}_i + \mu_i \cdot \mathbf{n}$$

Joining both previous equations, for each mooring line node i , it is obtained that $\mu_i = k - \mathbf{r}_i \cdot \mathbf{n}$, allowing to calculate \mathbf{r}'_i by replacing the term μ_i . Once \mathbf{r}'_i is obtained, it is possible to determine $d_{G,i}$ following its definition in Eq.(22) $d_{G,i} = (\mathbf{r}_i - \mathbf{r}'_i) \cdot \mathbf{n}_{S,i} = \mu_i \mathbf{n} \cdot \mathbf{n} = \mu_i$.

To sum up, if the seabed structure forms an inclined plane, the searched terms $d_{G,i}$ defined in Eq.(22) and $\mathbf{d}_{P,i}$ in Eq.(21) are defined as follows:

$$\text{Inclined plane} \begin{cases} \mathbf{d}_{P,i} &= \mathbf{n} \\ d_{G,i} &= \mu_i \end{cases} \quad \forall i \in \{0, \dots, N-1\}.$$

Figure 8 shows the process of projected a mooring line node in both a horizontal and an inclined seabed.

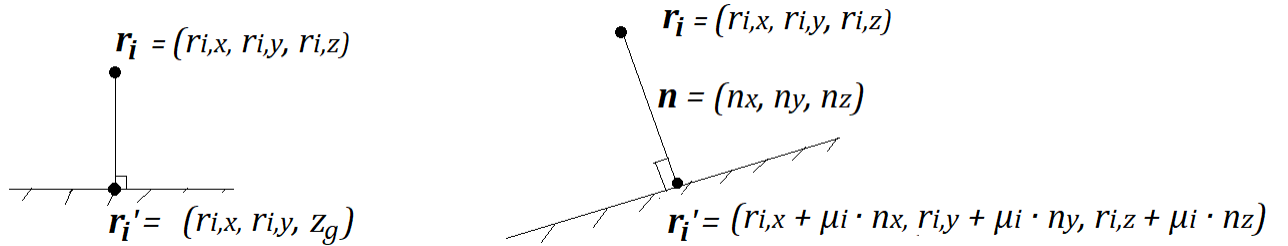


Figure 8: Mooring line node \mathbf{r}_i and its projection \mathbf{r}'_i in two different seabeds. On the left, an horizontal seabed is shown, at height z_g . On the right, an inclined seabed.

4.2.3 General case: Complex bathymetry

When the seabed surface is neither horizontal or plane, several difficulties appear. The different steps to follow are described below.

1) Interpretation of the seabed

The first concern may be the interpretation of the seabed surface, which can be carried out by triangulating the seafloor surface. In order to avoid an unnecessary computational cost, the surface should be described with the least triangles needed.

In order to construct the triangulation, the seabed surface must be firstly described by several points. Then, a triangulation using all the mentioned points as vertexes of different triangles is created.

2) Ensuring continuity in the projection algorithm

A second problem to treat is the necessity of obtaining a projection direction which is well-defined and varies continuously in order to avoid computational problems in the calculus of the jacobian needed for the temporal simulation.

The proposed method uses an algorithm to project into a triangulated surface (in this case, the seabed surface) developed by Orazi and Reggiani (2020) based on the vertex normals. Given a certain vertex of the triangulation V , its vertex normal is defined as the average of the normals of each triangle that has V as its vertex. Between the two normals of the triangles, the one pointing upwards, (to the sea level) is used. In Figure 9, it is shown an example.

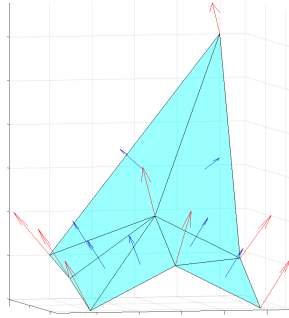


Figure 9: In blue, the normals for each triangle. In red, the vertex normals for each vertex.

The interest of using vertex normals instead of the normals of each triangle is that they ensure a continuous variation of the projection of direction, whereas with the normals of each triangle, not all the points are ensured to be projected. An example of this situation is represented in Figure 10



Figure 10: The left image shows the problem of using the normal vectors of the triangles forming the triangulation, painted in blue. The point A will be projected in the triangle T_1 whereas the point C will be projected in triangle T_2 . However, the projection of point B is not well defined. On the other hand, the right image shows the direction of projection that will be developed in this method, painted in green, which is based on normal vertexes, painted in blue. It can be seen that it varies continuously.

3) Reducing the computational cost of projecting in a triangulation constructing a change of frame matrix for each triangle

Orazi and Reggiani (2020) also conclude in their work that it is computationally profitable to construct a change-of-frame matrix G for each of the triangles that form the triangulation of the seabed surface. G lays the chosen triangle into the XY plane before starting the projection process, as Figure 11 shows. In order to achieve this, G is constructed by rotations and translations.

By laying the triangle into the XY plane, the projection process is much easier. For example, the previously introduced term $d_{G,i}$ can be easily calculated now. If it is found that the node i must be projected into a certain triangle of the seabed triangulation, with G being the matrix which lays the triangle into the XY plane, $d_{G,i}$ is the z-coordinate of the obtained point once both the triangle and the point have been multiplied by G , that is $d_{G,i} = (G\mathbf{r}_i)_z$.

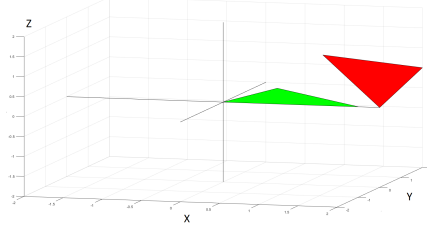


Figure 11: Matrix G converts the red triangle into the green one, laying it to the XY plane.

G and G^{-1} must be constructed and saved for each of the triangles which form the triangulation and describes the seabed surface. G allow to move to the change-of-frame where the triangle lays on the XY plane whereas G^{-1} will be used to return to the usual system of reference.

4) Projection process

To be able to project a mooring line node on the triangulation which describes the seafloor surface, it is firstly necessary to calculate in which triangle it has to be projected. Therefore, the projection process starts by selecting a mooring line node \mathbf{r}_i and one of the triangles which describe the seafloor surface. The line node is moved to the layed triangle change-of-frame with the matrix G for that triangle. The next step is to check whether the mooring line node has to be projected into the selected triangle or not. If it is not the case, another triangle is selected and the process is repeated until the desired triangle is found. The whole process followed in this section is based on Orazi and Reggiani (2020).

4.1) Checking if a point should be projected in a certain triangle

Let \mathbf{r}_i the mooring line node to be projected and T the triangle in which it wants to be checked whether \mathbf{r}_i must be projected there or not. T has vertexes $\{\mathbf{V}_j\}_{j=0,1,2}$ and unitary normal vertexes of $\{\mathbf{n}_j\}_{j=0,1,2}$. The first step is to construct another triangle T_{point} parallel to T which contains \mathbf{r}_i and with vertexes $\{\mathbf{U}_j\}_{j=0,1,2}$, as it can be sen in Figure 12. The new triangle vertexes can be expressed by:

$$\mathbf{U}_j = \mathbf{V}_j + k\mathbf{n}_j \text{ with } j \in \{0, 1, 2\}$$

where k is a scalar that represents the distance between the triangle in the seabed surface T and the one constructed T_{point} containing the point to project, \mathbf{r}_i .

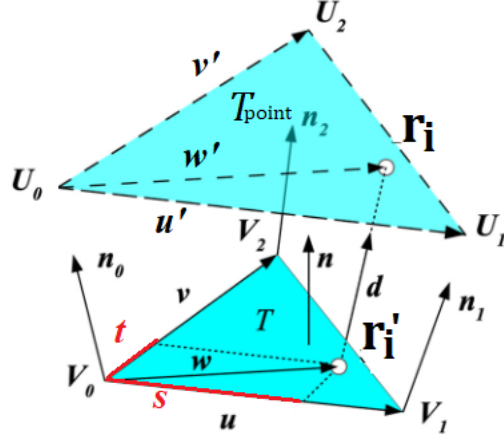


Figure 12: The point to project is \mathbf{r}_i and the seabed surface triangle in which it is desired to be projected is T , with vertexes $\{\mathbf{V}_j\}_{j=0,1,2}$ and normal vertexes $\{\mathbf{n}_0\}_{j=0,1,2}$. A parallel triangle to T which contains \mathbf{r}_i is constructed, T_{point} , with vertexes $\{\mathbf{U}_j\}_{j=0,1,2}$. The image has been taken from Orazi and Reggiani (2020).

Then, the vectors \mathbf{u}' , \mathbf{v}' and \mathbf{w}' that are described in Figure 12, are defined the following way:

$$\begin{aligned}\mathbf{u}' &= \mathbf{U}_1 - \mathbf{U}_0 \\ \mathbf{v}' &= \mathbf{U}_2 - \mathbf{U}_0 \\ \mathbf{w}' &= \mathbf{r}_i - \mathbf{U}_0\end{aligned}$$

These vectors allow to define the barycentric coordinates (s, t) which define the position of \mathbf{r}_i in the new created triangle T_{point} :

$$\mathbf{w}' = \mathbf{u}'s + \mathbf{v}'t$$

which must be verified for each component, defining a system of linear equations where the solution gives the values of s and t .

The point \mathbf{r}_i will be contained into the new constructed triangle T_{point} if its barycentric coordinates accomplish the following condition:

$$\begin{cases} s & \geq 0 \\ t & \geq 0 \\ s + t & \leq 1 \end{cases}$$

In this case, \mathbf{r}_i will be projected in T so \mathbf{r}'_i , the projection of the point \mathbf{r}_i , will be contained in T .

4.2) Calculating the projected point

By Figure 12, it can be seen that barycentric coordinates (s, t) of the projected point \mathbf{r}'_i in T will remain the same as previous calculated for the point to project \mathbf{r}_i in T_{point} . The coordinates of \mathbf{r}'_i can be easily obtained by using these set of vectors $\{\mathbf{u}, \mathbf{v}\}$ defined as follows:

$$\begin{aligned}\mathbf{u} &= \mathbf{V}_1 - \mathbf{V}_0 \\ \mathbf{v} &= \mathbf{V}_2 - \mathbf{V}_0\end{aligned}$$

Giving

$$\mathbf{r}'_i = \mathbf{V}_0 + \mathbf{u}s + \mathbf{v}t$$

providing the coordinates of \mathbf{r}'_i . The direction of projection will be \mathbf{d} in Figure 12 and can be calculated by

$$\mathbf{d} = \mathbf{r}'_i - \mathbf{r}_i \quad \forall i \in \{0, \dots, N-1\}.$$

Finally, it is obtained that $\mathbf{d} = \mathbf{d}_{P,i}$ for each mooring line node, obtaining all the needed terms to calculate the mooring dynamics in a complex bathymetry. \mathbf{d} is a good approximation of the seabed surface normal, although it is not the normal of the triangle in which the point has been projected, as it can be seen in Figure 12.

To sum up, when the seafloor has an irregular seabed surface, the desired terms $d_{G,i}$ defined in Eq.(22) and $\mathbf{d}_{P,i}$ in Eq.(21) are calculated as follows:

$$\text{Irregular bathymetry} \quad \begin{cases} \mathbf{d}_{P,i} = \mathbf{V}_0 + \mathbf{u}s + \mathbf{v}t - \mathbf{r}_i \\ d_{G,i} = (G\mathbf{r}_i)_z \end{cases} \quad \forall i \in \{0, \dots, N-1\}$$

with the obtained G , \mathbf{u} , \mathbf{v} , \mathbf{V}_0 for the triangle in which the mooring line node \mathbf{r}_i is projected and (s, t) the barycentric coordinates of the projected point in that triangle.

4.2.4 Application: Calculation of ground normal and friction forces.

The previously introduced terms $d_{G,i}$ and $\mathbf{d}_{P,i}$ are used to describe friction \mathbf{f}_f and ground normal \mathbf{f}_n forces which were introduced in Eq.(2) in any type of seafloor.

Ground normal force model \mathbf{f}_n .

The ground normal force is perpendicular to the seafloor surface and should only be considered when the mooring line touches the seafloor, which introduces a step discontinuous function. However, its mathematical description has to be smooth in order to avoid numerical divergences.

To solve this problem, a tool able to smooth a step function $f(x)$ was developed. The step function can be described as follows:

$$f(x) = \begin{cases} f_0 & \text{if } x < p \\ f_f & \text{if } x \geq p \end{cases}$$

Let $f_{sm}(x)$ be the smoothed version of the function $f(x)$. The idea is to approximate the discontinuity by a polynomial in a interval $[p_0, p_f]$ (being $p_f = p$ the discontinuity), obtaining the situation presented in Figure 13:

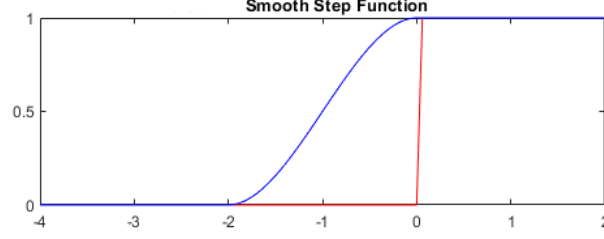


Figure 13: In red, a step function $f(x)$ with a discontinuity in $p = 0$. The step function values $f_0 = 0$ at $x < 0$ and $f_f = 1$ at $x \geq 0$. In blue, the smoothed function which approximates the step function by a polynomial in the interval $[p_0 = -2, p_f = 0]$.

The physical meaning of introducing a step function in the ground normal force is that it starts acting gradually, instead of varying from zero to a certain value in the exact moment in which the mooring line touches the seafloor.

The polynomial of approximation has to verify four boundary conditions: two of them are related to the function in the extremes of the interval, $f_{sm}(p_0) = f_0$ and $f_{sm}(p_f) = f_f$. The other two refer to having null derivatives in the limits of the interval, $\frac{df_{sm}(p_0)}{dx} = 0$ and $\frac{df_{sm}(p_f)}{dx} = 0$.

As there are four boundary conditions, the step discontinuity can be modelled by a third degree polynomial defined in the interval $[p_0, p_f]$. In other words,

$$f_{sm}(x) = \begin{cases} f_0 & \text{if } x < p_0 \\ ax^3 + bx^2 + cx + d & \text{if } x \in [p_0, p_f] \\ f_f & \text{if } x > p_f \end{cases}$$

Applying the boundary conditions to the polynomial defined in the interval $[p_0, p_f]$ leads to the following system of equations

$$\begin{cases} ap_0^3 + bp_0^2 + cp_0 + d = f_0 \\ ap_f^3 + bp_f^2 + cp_f + d = f_f \\ 3ap_0^2 + 2bp_0 + c = 0 \\ 3ap_f^2 + 2bp_f + c = 0 \end{cases}$$

where the coefficients (CF) of the polynomial can be obtained by solving the system $A*CF = b$, where the following matrices are introduced:

$$A = \begin{pmatrix} p_0^3 & p_0^2 & p_0 & 1 \\ p_f^3 & p_f^2 & p_f & 1 \\ 3p_0^2 & 2p_0 & 1 & 0 \\ 3p_f^2 & 2p_f & 1 & 0 \end{pmatrix}; \quad b = \begin{pmatrix} f_0 \\ f_f \\ 0 \\ 0 \end{pmatrix}; \quad CF = \begin{pmatrix} a \\ b \\ c \\ d \end{pmatrix}.$$

From now on, the following notation will be considered:

$$f_{sm}(x) = sm(x, p_0, f_0, p_f, f_f).$$

This smoothed function is introduced in the description of the ground normal force model by a term α , as it can be seen in Eq.(24). α is a scalar coefficient which varies continuously from 0 to 1 that multiplies the ground normal force depending on the ground penetration of the mooring line node. In other words, α is a smoothed function which evaluates the ground penetration for a certain mooring line node, $f_{sm}(d_{G,i})$. It is considered that, when the lowest part of the mooring line touches the seafloor ($d_{G,i} = -d/2$, being d the mooring diameter), the ground normal force starts to act gradually until it reaches its full potential when the center of the mooring line touches the seafloor ($d_{G,i} = 0$). Therefore,

$$\alpha = sm(d_{G,i}, -d/2, 0, 0, 1). \quad (23)$$

Introducing α converts the ground normal force into a smooth function, which improves the behaviour of the numerical method and avoids divergences.

The description used to model ground normal force is based on a combination of Palm et al. (2013) and Trubat et al. (2020) ground normal force models. However, both articles describe its models in a horizontal seabed, so the terms $d_{G,i}$ and $\mathbf{d}_{P,i}$ had to be introduced in their equations, allowing to consider the interaction between the mooring line and an irregular seafloor. In addition, the provided description has been modelled with smooth coefficients that improve the computational behaviour of the simulation.

The expression obtained for the ground normal force in a certain mooring line node i is the following:

$$\mathbf{f}_n = \alpha(\mathbf{f}_{spring} + \mathbf{f}_{damp} + \mathbf{f}_{usual}) \quad (24)$$

where α was described in Eq.(23) and

- $\mathbf{f}_{spring} = -dG_K d_{G,i} \mathbf{d}_{P,i}$ is the force which models the mooring line as an spring.
- $\mathbf{f}_{damp} = -2\sqrt{G_K d \gamma_0} \min(0, v_n) \mathbf{d}_{P,i}$ is the term which quantifies the damping of the spring.
- $\mathbf{f}_{usual} = \|p_n\| \mathbf{d}_{P,i}$ is the common approach to the normal force, which depends on the effective weight.

Let's start by defining the terms which have taken from Palm et al. (2017) and Trubat et al. (2020) models. d and γ_0 are defined as in Eq.(1) and G_K is the ground normal stiffness per unit area.

Apart from the previously introduced $\mathbf{d}_{P,i}$ and $d_{G,i}$, the next terms have been newly developed in order to consider the interaction with a variable seafloor:

- v_n is the velocity normal to the seafloor $v_n = \mathbf{v} \cdot \mathbf{d}_{P,i}$, where v is the total mooring node velocity.
- $\|p_n\|$ is the normal component of the effective weight and is given by the expression:

$$\|p_n\| = (\gamma_W - \gamma_0) g \mathbf{e}_3 \cdot \mathbf{d}_{P,i}$$

with $g = 9.8 \text{ m/s}^2$ the scalar value of Earth's gravity and γ_W described as in Eq.(29).

Friction force model \mathbf{f}_f

The friction force is contained in the plane of the seabed and it opposes the movement of the mooring line. The model used is based on Devries (2018).

$$\mathbf{f}_f = \begin{cases} -C_k \|\mathbf{f}_n\| \frac{\mathbf{v}_\pi}{v_c}, & \text{if } \|\mathbf{v}_\pi\| < v_c. \\ -C_k \|\mathbf{f}_n\| \frac{\mathbf{v}_\pi}{\|\mathbf{v}_\pi\|}, & \text{otherwise.} \end{cases} \quad (25)$$

being C_k the kinetic friction coefficient, v_c a velocity threshold (a scalar, usually taken as $v_c = 0.01m/s$) and \mathbf{f}_n the previous calculated normal force. \mathbf{v}_π is the velocity contained in the seafloor surface plane, and can be obtained by $\mathbf{v}_\pi = \mathbf{v} - v_n \mathbf{d}_{P,i}$.

As the friction force directly depends on the ground normal force, which is a smooth function, there is no need to apply any smoothed coefficient to this formulation.

Finally, the description of ground normal and friction forces allows to consider the interaction between an irregular seabed surface and the mooring line in the numerical simulation, which was the main objective of this work.

4.3 Initial condition problem: Newton-Armijo

The mooring simulation is based on a wave equation formulation and therefore depends on two initial conditions: initial mooring line positions ($\mathbf{r}(0, s)$) and velocities ($\frac{d\mathbf{r}(0, s)}{dt}$), as it was discussed in section 2. However, the initial velocities are considered to be zero (static approach) so the initial condition problem is reduced to find the initial mooring line positioning $\mathbf{r}(0, s) = \mathbf{g}(s)$.

Before implementing an irregular seabed surface, a catenary between the fairlead and the anchor was used as a initial condition. However, this situation does not represent a reliable behaviour when the seafloor is not flat because there could be buried parts, as Figure 14 shows, which will increase tensions as well as providing an unrealistic position of the mooring line. Therefore, the initial condition was changed to the static equilibrium of the mooring line.

- Newton's method

The static equilibrium is found by Newton's iterative method, which is capable of solving non-linear systems in the form $\mathbf{F}(\mathbf{r}) = \mathbf{0}$ by approximating them to a linear system, where \mathbf{r} is the vector with the mooring line nodes initial positions. Its size is $3N$, being N the number of nodes in which the mooring line has been discretized and 3 the number of dimensions. In other words,

$$\mathbf{r} = (r_{0,x}, r_{0,y}, r_{0,z}, \dots, r_{N-1,x}, r_{N-1,y}, r_{N-1,z}).$$

$\mathbf{F}(\mathbf{r})$ is again a $3N$ sized vector which contains the forces in those positions.

Newton's method starts by an initial approach $\mathbf{r}^{(0)}$ in which a good convergence is ensured. This is achieved by choosing $\mathbf{r}^{(0)}$ as a catenary between the anchor and the fairlead. Other initial approaches were tried, such as the line between the fairlead and the anchor. However,

by using these other mooring line positionings as initial points in Newton-Armijo method, the static equilibrium was found at the inverse catenary as it can be seen in Figure 15, which is not realistic.

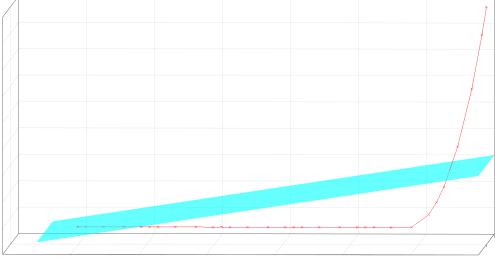


Figure 14: The static approach of a catenary between the fairlead and the anchor using a sloped seabed (blue) can bury the mooring line (red), as it happens in the image, which is not realistic.

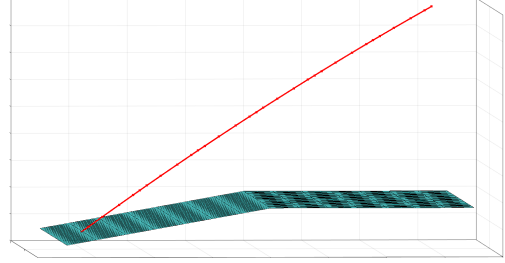


Figure 15: The initial mooring line positioning which Newton's method uses as initial point ($\mathbf{r}^{(0)}$) should be carefully selected in order to avoid reaching the static equilibrium in an inverse catenary.

Then, the method starts iterating and generating other points by following a descent direction that approaches to the solution. The iterations in Newton's method are constructed the following way:

$$\mathbf{r}^{(k+1)} = \mathbf{r}^{(k)} + \mathbf{d}^{(k)} \quad (26)$$

being $\mathbf{d}^{(k)}$ the descendent direction, calculated by solving the following system:

$$\mathbf{JF}(\mathbf{r}^{(k)})\mathbf{d}^{(k)} = -\mathbf{F}(\mathbf{r}^{(k)})$$

where \mathbf{JF} is the jacobian approximated by finite differences:

$$\mathbf{JF}(\mathbf{r}^{(k)}) \approx \left(\begin{array}{ccc} \frac{\mathbf{F}(\mathbf{r}^{(k)}+h\cdot\mathbf{e}_1)-\mathbf{F}(\mathbf{r}^{(k)})}{h} & \frac{\mathbf{F}(\mathbf{r}^{(k)}+h\cdot\mathbf{e}_2)-\mathbf{F}(\mathbf{r}^{(k)})}{h} & \dots & \frac{\mathbf{F}(\mathbf{r}^{(k)}+h\cdot\mathbf{e}_{3N})-\mathbf{F}(\mathbf{r}^{(k)})}{h} \end{array} \right)$$

which shows that the Jacobian is a $3N \times 3N$ matrix. h is the parameter of finite differences which was chosen to be 10^{-12} .

Newton's maximum number of iterations must be restricted in order to avoid infinite loops when no convergence is achieved: it was set to 30. If in 30 iterations the solution is not found, the method will throw an exception and stop. The solution is considered to be found when the iterations start being close:

$$\text{Newton's method convergence criteria} \left\{ \begin{array}{ll} \|\mathbf{r}^{(k+1)} - \mathbf{r}^{(k)}\| < 10^{-6} & \text{Absolute error} \\ \text{or} & \\ \frac{\|\mathbf{r}^{(k+1)} - \mathbf{r}^{(k)}\|}{\|\mathbf{r}^{(k)}\|} < 10^{-3} & \text{Relative error} \end{array} \right. \quad (27)$$

- Introduction of Armijo's variable step.

The descendent direction can be multiplied by a scalar called step that controls the distance between two consecutive iterations. In Eq.(26), the step used is 1, which may define a too

large separation between two interactions, as Figure 16 shows. The convergence was highly improved when Armijo's variable step $\rho^{(k)}$ (being k the number of iteration) was added to Eq.(26), transforming it to the following:

$$\mathbf{r}^{(k+1)} = \mathbf{r}^{(k)} + \rho^{(k)} \mathbf{d}^{(k)}$$

where $\rho^{(k)}$ is calculated in each iteration by finding a value which satisfies the following condition:

$$\|\mathbf{F}(\mathbf{r}^{(k)} + \rho^{(k)} \mathbf{d}^{(k)})\| \leq (1 - \sigma \rho^{(k)}) \|\mathbf{F}(\mathbf{r}^{(k)})\| \quad (28)$$

where $\rho^{(k)} = 2^{-n}$ with $n \in \mathbb{N}$ and $\sigma = 10^{-4}$. In order to find the value $\rho^{(k)}$ which satisfies the condition in Eq.(28), n subiterates increasing from 0 until the desired condition is satisfied, with a maximum number of 12 subiterations allowed.

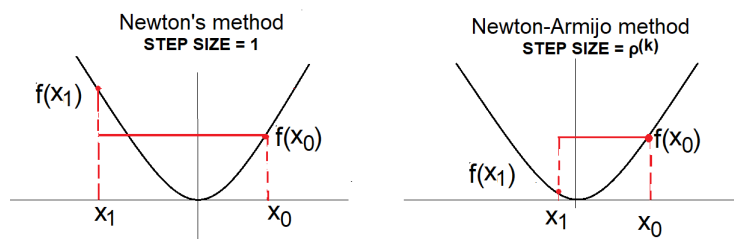


Figure 16: Armijo's variable step improvement shown in a specific example. In the left image, the iteration has been generated with the Newton basic method defined in Eq.(26). The direction is descent, but the step is too big, moving away from the solution. The right image generates its iterations using the Armijo's variable step described in Eq.(28), which is shorter and allows to approach to the minimum in a lower number of iterations.

5 Results

This section is specially important because it allows to verify the theoretical work previously developed. In this work, only two different ways of validating the results will be considered, but there have been more methods used that can be consulted in the work developed (Desiré et al., 2022), even experimental tests which required lab work performed by several technicians of *IHCantabria*.

5.1 Comparison between the analytic and simulation results

In order to evaluate the agreement between the analytical and the numerical method, a first experiment that consists of solving the static specific solution described in subsection 3.1 with the numerical method was performed. As the particular situation studied was defined by a mooring line partially laying in a seafloor with an inclined plane structure, this method also allows to verify the projection method constructed for inclined and flat seafloors.

The first step is to adjust the needed parameters for the numerical simulation in order to imitate the particular situation desired, which are described as follows:

- The fairlead was imposed being static by defining its position vector as $\mathbf{r}_F(t) = \mathbf{0} \forall t$.
- The mooring line was restricted to be in the plane $Y = 0$, reducing its description to two dimensions.
- The projection algorithm used was the specific one developed for inclined plane seafloor structures described in 4.2.2.
- The ground has been treated as impenetrable and the mooring line as inextensible by increasing certain coefficients in the models which describe the forces. Although explaining these coefficients is out of the limits of the work, a detailed description can be found in the article developed (Desiré et al., 2022).

In order to reproduce the analytic solution provided by Eq.(17), the characteristic length of the catenary (λ) must be calculated, which can be done using Eq.(7). This expression depends on the mooring line weight per unit of length in the water γ_W , that can be calculated by applying Archimedes principle:

$$\gamma_W = \gamma_0 - \rho_W \pi \frac{d^2}{4} \quad (29)$$

where ρ_W is the water density, d is the mooring diameter and γ_0 is the mooring line per unit of weight. These parameters are provided as external parameters to the simulation, and its values are shown in Table 1.

Abbreviation	Parameter	Value
\mathbf{r}_0	Anchor Position (m)	$[-601.4, 0, -83.5]$
L	Length (m)	635
γ_0	Weight per unit of length (kg/m)	835.4
d	Line diameter (m)	0.3539
ρ_W	Water density (kg/m^3)	1025
G_K	Ground normal stiffness per unit area (N/m^3)	$3 \cdot 10^{14}$
v_c	Velocity threshold (m/s)	0.01
C_K	Kinetic friction coefficient	0.3

Table 1: Mooring line characterization and coefficients used to calculate ground normal force in Eq.(24) and friction force in Eq.(25).

Once the needed parameters have been set, the results for both numerical and analytical methods can be obtained and compared. Two different types of comparisons will be performed: mooring line positioning and tension at the fairlead.

5.1.1 Tension at the fairlead comparison

As it was previously discussed, the tension at the fairlead is an important quantity because it can be easily measured experimentally. Eq.(13) provides an analytical expression to obtain it, while the one obtained numerically is an output of the execution of the code. Both of them were compared, obtaining the following results:

H (kN)	T_N (kN)	T_A (kN)	$ T_N - T_A $ (kN)	δT
3500	5369	5373	4	0.0007
3700	5184	5188	4	0.0008
4000	4915	4912	3	0.0006
4300	4633	4637	4	0.0009
4500	4453	4454	1	0.0002

Table 2: Horizontal external force H used to calculate the analytical solution. T_N and T_A are the obtained fairlead numerical and analytical tensions, respectively. δT is the relative error, calculated by $\frac{|T_N - T_A|}{T_A}$.

The relative errors shown in Table 2 are all of them lower than 10^{-3} , showing great accordance between the results of the analytic and numerical solutions. It can be seen that there is certain inhomogeneity between the results, which leads to argue that those errors are introduced by Newton-Armijo convergence criteria detailed in Eq.(27), which allowed a magnitude of relative error of 10^{-3} , the same magnitude as the relative errors shown above.

5.1.2 Position comparison

The execution of the simulation leaves as an output the position of the mooring line nodes in which the mooring was discretized, that could be compared with the analytical solution obtained from Eq.(17). The results can be seen in Figure 17.

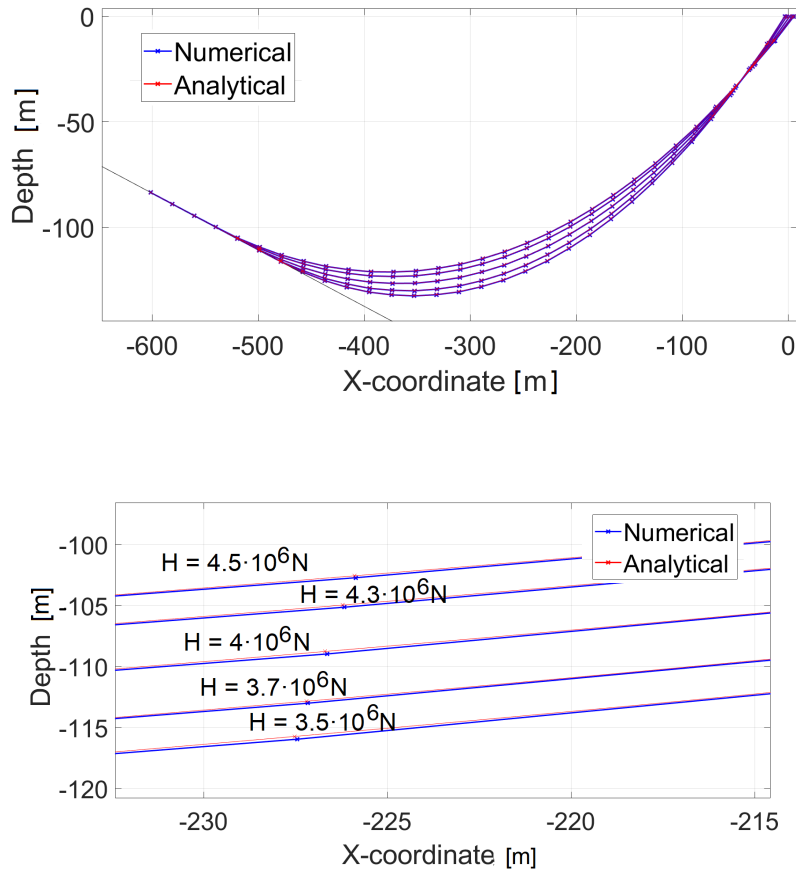


Figure 17: Comparative between the analytical expression (red) and the numerically obtained mooring line nodes positions (blue) for different values of external horizontal force H . The image below is a magnification of the above image which tries to make visible the differences between both methods.

Figure 17 shows an excellent accordance between two methods. In order to obtain a numerical comparison, the absolute differences between the positions of both methods were also shown in Table 3. However, as the number of mooring line nodes is 31, in order to avoid an excessive long table with the differences for all the nodes, only certain nodes have been discussed. The selected nodes correspond to the rounded value of the n -th percentile of the 31 of them, with $n \in \{10, 20, \dots, 90\}$.

$H(N)$ \ Node	2	6	9	12	16	19	22	25	29
$4.5 \cdot 10^6$	0.031	0.085	0.042	0.159	0.169	0.182	0.129	0.23	0.249
$4.3 \cdot 10^6$	0.014	0.051	0.039	0.162	0.185	0.187	0.148	0.237	0.255
$4 \cdot 10^6$	0.023	0.012	0.064	0.167	0.211	0.142	0.178	0.208	0.255
$3.7 \cdot 10^6$	0.014	0.123	0.029	0.178	0.177	0.2	0.125	0.255	0.275
$3.5 \cdot 10^6$	0.017	0.078	0.037	0.161	0.231	0.181	0.204	0.244	0.277

Table 3: Absolute difference (in meters) between the numerical and analytic results for certain mooring line nodes. The difference located in row i and column j , $\Delta(i, j)$, corresponds to the results obtained applying an external force H_i and is associated with the node j . It has been calculated as $\Delta(i, j) = \sqrt{\Delta_x(i, j)^2 + \Delta_z(i, j)^2}$, where $\Delta_x(i, j)$ is the absolute difference between the numerical and the analytical values of the X-positions of the j -th node for the external force H_i , and $\Delta_z(i, j)$ is the same quantity for the Z-positions.

Table 3 shows differences in the position between the numerical and the analytical solution of the order of centimeters. Regarding the total length of the mooring line, 635m (as it can be seen in Table 1), it leads to relative errors of the order of 0.01%, from it which can be concluded that the numerical method provides a very exact result.

However, Figure 17 shows that the numerical solution is always slightly below the analytical, instead of finding the irregular errors present in the fairlead tensions. This can be explained because the numerical simulation is not able to model perfectly inextensible moorings, as it would imply setting an external parameter to be infinity, which makes no sense computationally. The parameter must be a finite quantity, introducing certain error.

5.2 Qualitative tests

The previous comparison allowed to verify the accuracy of the projection method for seafloors with an inclined plane structure. However, the general projection algorithm constructed in 4.2.3 has not been analyzed yet. In order to verify this method, several numerical simulations with different seabed surfaces were performed. The idea is to compare graphically the position results provided by the numerical method with the seafloor surfaces.

The first approach is to analyze the numerical solution behaviour when different seabed surfaces with convex and concave changes in gradients were studied, obtaining the following results:

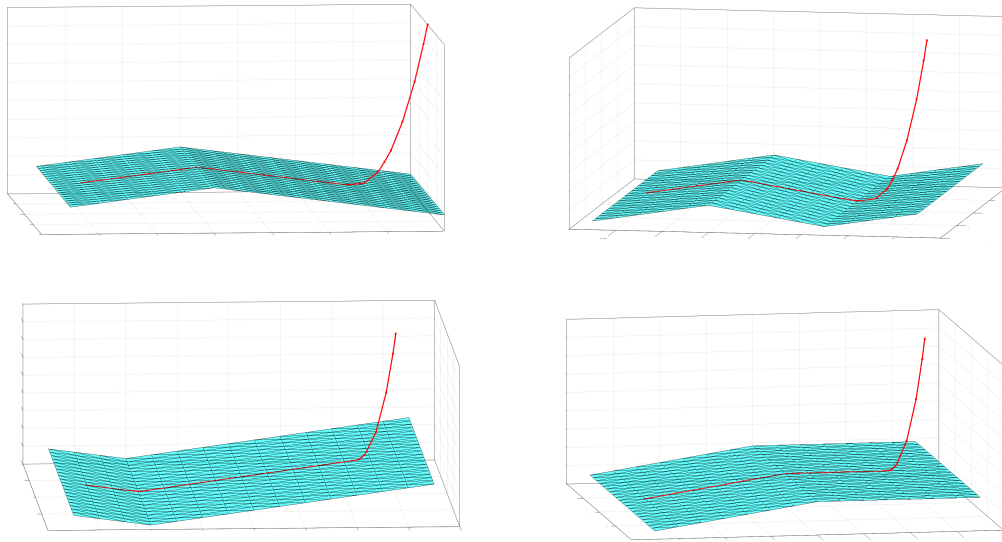


Figure 18: Graphical results of the mooring position $\mathbf{r}(t, s)$ (in red) in different seabed configurations (convex and concave). It can be seen that the mooring follows accurately the seabed surface in all cases. The projection method used was the general, described in 4.2.3. This method was based in a triangulation describing the seabed surface that has been painted in blue.

Graphically, it can be seen that the obtained positions $\mathbf{r}(t, s)$ are coherent with the seabed structure for all cases.

Then, a more complex seabed surface which was irregular along both X and Y axis has also been studied. In this case, an extra comparison has been done. Figure 19 shows the difference between the obtained positions for the numerical method equipped with the projection algorithm and the one which was previously implemented, that was only able to consider flat seabeds.

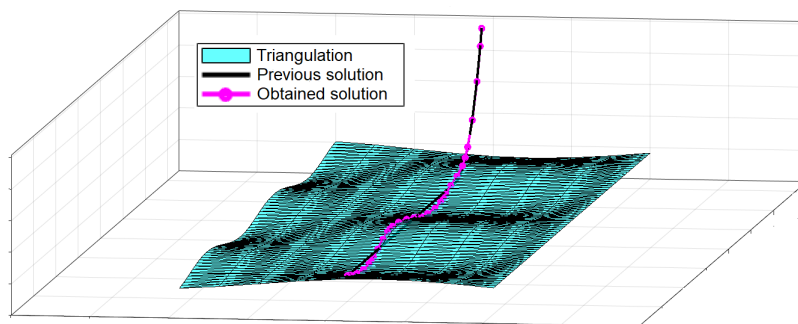


Figure 19: Graphical result of the mooring position obtained $\mathbf{r}(t, s)$ (in purple) by the numerical simulation when the projection tool developed in 4.2.3 is used. In black, the results obtained when the projection tool is not used. In blue, the triangulation describing the seabed surface.

Figure 19 showed how the obtained positions when the projection method was not used do not follow the seabed surface, while in the case where the projection method was used, it did. Therefore, the positions are more realistic in this last case.

Furthermore, not using the projection method leads to obtain buried parts of the mooring line which are not realistic, as they are not produced when the general projection algorithm is used. The buried parts will cause an increase in the mooring line tensions that does not represent the real behaviour and therefore worsens the numerical simulation.

6 Conclusions

The present work describes an optimal projection new method able to simulate a mooring line in a seafloor surface described by an horizontal plane, inclined plane or a complex bathymetry. The developed method allows to evaluate friction and ground normal forces in any seabed structure, improving the accuracy of the simulations specially in deep waters, where the seabed usually describes a sloped configuration.

The work started with the introduction of the mooring line dynamics as a PDE system restricted to certain boundary and initial conditions, leading to a wave type problem. Then, the mooring line was subject to a particular static situation described by Batista and Perkovic (2019) in which the seafloor was an inclined plane, which could be solved analytically. The solution was obtained by constructing a parameterization based on arc length coordinates. However, the general non-static case could not be solved analytically. The problem was homogenized and later solved by a finite element method (FEM) based on Galerkin continuous method which uses first order functions in its basis. The final result of applying this method was a system of second order ODEs that were reduced to first order.

The novel part of this work was the developed continuous projection tool, which operated differently depending on the seabed surface: horizontal, inclined plane or irregular. The projection process in the two first types of seafloors was based in a point-to-plane projection, which allowed to reduce the computational cost in those simpler cases. For complex bathymetries, it was necessary to construct a triangulation describing the seafloor surface. The projection method used was based on vertex normals which provide method's continuity, as Orazi and Reggiani (2020). Finally, the projection tool calculated the direction of projection and the penetration depth, terms which were used to model friction and ground normal forces. These forces depend on the seafloor structure, so introducing these terms greatly improved the precision of the simulation when a seafloor distinct from the flat one is considered.

The initial condition of the problem was defined as the static equilibrium, instead of the previously used catenary between the mooring line extremes. The static equilibrium was found with Newton's iterative method improved by using the variable Armijo step.

Finally, the particular static situation used to obtain the analytical solution was solved numerically and the positions and tensions results of both methods were compared. The accordance between them is excellent: the relative differences found in the positions are of order of 0.01% and are attributed to not obtaining a complete inextensible mooring line numerically, while the relative differences between the tensions are lower than 0.1%, which is the criteria of convergence used in Newton-Armijo method. The obtained results verify not only the numerical method but also the projection tool developed for inclined planes. In order to validate the general projection method, several qualitative tests which included irregular bathymetries were performed, obtaining a good coherence between the mooring line positions and the seabed structure.

Further research can be oriented to improve the numerical method used by using discontinuous Galerkin method in FEM formulation instead of the Galerkin continuous method

which was used in this work. Discontinuous Galerkin was applied by Palm et al. (2017) in mooring line simulations, obtaining really accurate results. In addition, the FEM basis functions could be constructed with higher order polynomials.

Other possible point to improve is the friction model, as it does only include a unique friction coefficient and does not differentiate between static and dynamic friction. Stick and slip model described in Marques et al. (2016) is a good candidate because it depends on only four external parameters, easing the experimental calibration process, and models with accuracy the transition between static and dynamic friction. In addition, when an irregular bathymetry is considered, the friction should not be described by the same coefficients in all of its directions. This is known as anisotropic behaviour. Friction force is defined in the seabed plane, however, the anisotropic model differences between tangential and perpendicular friction force components by describing them with different friction coefficients.

7 Additional work

In this section, a brief description of the work developed that has not been included in the document is presented.

7.1 Implementation

The developed work can be divided in two different parts: the theoretical one, which has been explained in the presented document, and a implementation part which was carried out during a three-month full-time internship in *IHCantabria* (385h). The institution had already developed a FEM numerical method implemented on C++ able to simulate three dimensional mooring lines in an horizontal seafloor.

To make the method capable of evaluating the interaction with the seabed as explained in the work, the following implementation was incorporated to the already existing code:

- Creation of a new class: *Seafloor*

The seafloor class is based in a system of inheritance in which the defined subclasses are horizontal, inclined and irregular. All the subclasses share the existence of the projection method described in subsection 4.2 as well as a reading method which allows to interpret the provided inputs. However, for each of the subclasses, the mentioned algorithms are defined differently.

It should be mentioned that the projection method in the irregular bathymetry subclass has a lot of submethods defined. For example, there is a submethod which allows to calculate a triangulation from a cloud of points as well as other that calculates the normal vertexes for each of the triangles.

One of the most difficult submethods to design and implement was the one able to calculate and store the change-of-frame G matrices described in 4.2.3, as it calculates and constructs the needed rotations and translations which lay each of the existing triangles in the XY plane.

- Implementation of ground normal and friction forces model in the existing description of the mooring dynamics.

IHCantabria had a previous code which considered several of the external forces described in Eq.(2). The newly developed models of ground normal force (see Eq.(24)) and friction force (see Eq.(25)) were computationally incorporated to the existing code in the class *Lines*, ensuring that they were smooth, as it was previously discussed, and therefore provided a good convergence.

- Substituting the previous initial condition by the static equilibrium found by Newton-Armijo.

As it was explained in subsection 4.3, the previous initial condition was a catenary between the anchor and the fairlead, which has been substituted by a static equilibrium found by

Newton-Armijo iterative method. This was performed following the numerical implementation of Newton-Armijo at Kelley (2003), and it was performed in another different class called *Solver*.

- Creation of a graphical tool able to visualize the mooring line positioning and the seabed

The images shown in the qualitative tests exposed in Subsection 5.2 were generated with this constructed tool able to interpret the code output as well as the description of the seafloor, which is a code input. As this part only works with inputs and outputs, it does not need to be done inside the C++ code, so it was decided to be implemented in Matlab. It is also able to generate videos.

Finally, it should be mentioned that the execution time of this code is really high: some of the tests performed to check whether the method was providing a good numerical convergence took more than 4 days. This added an extra difficulty to the development of the implementation.

7.2 Article

The presented work is the basis of an article which has already been submitted to the journal *Ocean Engineering* (Desiré et al., 2022). In the article, there were several additional considerations that can be summed up as follows:

- The strain $e(t, s)$ in the description of the mooring line dynamics introduced in 2.3 was not treated as zero.
- The obtained results were also validated against several experimental tests developed with different seabed configurations, obtaining a great accordance. Those tests were performed by several technicians at *IHCantabria*. Some of them carried out the experimental set-up while others worked on the calibration of external coefficients.
- The projection method developed for complex bathymetries in 4.2.3 was improved by starting to iterate from the triangles with the closest barycenter to the mooring line node in question, achieving an improvement of the computational time required when the number of triangles is high.
- The article includes a method of verification that consists in performing a comparative between the three projection methods studied: the ones developed for flat, inclined plane and irregular seabed surfaces. The idea was to take an irregular inclined seafloor surface and simulate the mooring with the general projection method. Later, the seabed surface was interpolated by an inclined plane and the mooring line was simulated with the developed projection method for inclined surfaces. Finally, the seafloor was approximated by a flat surface with the mean depth of the points which described the irregular initial surface and the numerical simulation was performed with the algorithm developed for flat surfaces.
- The number of nodes in which the mooring should be discretized depends on the seabed surface. If there are narrow irregularities, not only the triangulation of the

seabed should be done carefully, but also the discretization of the chain, which must be fine enough to be able to consider interactions. Otherwise, a situation similar to the one described in Figure 20 can appear. However, describing the mooring line with a too large amount of nodes will cause an excessive increase in the computational cost required by the FEM method.

Therefore, the article includes a sensibility analysis with respect to the number of nodes which ensures a correct interpretation of the seabed and mooring line interaction.

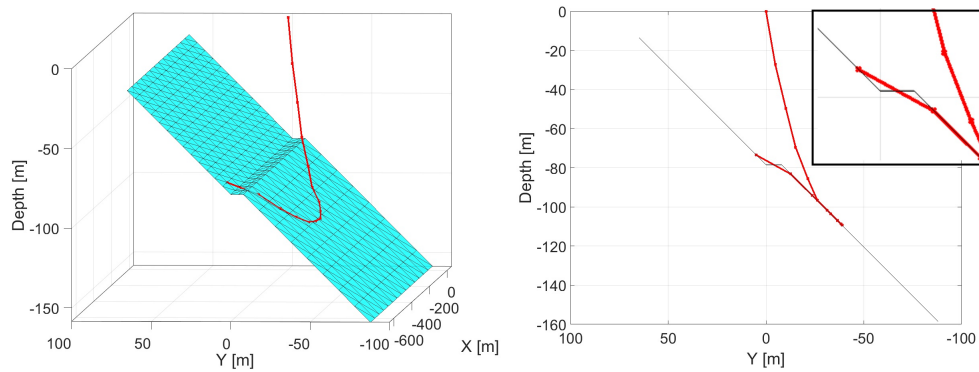


Figure 20: If the number of mooring line nodes is too small, some seabed irregularities may not be considered, leading to a bad numerical simulation. However, overincreasing the mooring line nodes will cause a huge increase in the computational cost of the projection algorithm.

References

- Aamo, O., Fossen, T., 2000. Finite element modelling of mooring lines. *Math. Comput. Simul.* **53**, pp. 415–422. doi:[https://doi.org/10.1016/S0378-4754\(00\)00235-4](https://doi.org/10.1016/S0378-4754(00)00235-4).
- Batista, M., Perkovic, M., 2019. Computation of mooring chain with the touchdown on an inclined seabed. *J. Mar. Eng. Technol.* **21**, pp. 9–22. doi:<https://doi.org/10.1080/20464177.2019.1572059>.
- Burden, R., Faires, D., 2013. *Análisis Numérico*. 10th edition. México D.F.: Cengage Learning Editores .
- Desiré, P., Rodríguez-Luis, A., Guanche, R., 2022. Simulation of mooring lines in complex bathymetries using a finite element method. *Ocean Eng.* Sometido a publicación.
- Devries, K. and Hall, M., 2018. Comparison of seabed friction formulations in a lumped-mass mooring model. *ASME 2018 1st International Offshore Wind Technical Conference. Proceedings: Nov. 4-7, 2018, San Francisco, CA*. doi:10.1115/IOWTC2018-1099.
- Feng, A., Kang, H., Zhao, B. and Jiang, Z., 2020. Two-dimensional numerical modelling of a moored floating body under sloping seabed conditions. *J. Mar. Sci. Eng.* **8**(6), pp. 389. doi:10.3390/jmse8060389.
- Flexcom, 2021. 3D Seabed Profile. URL: https://flexcom.fea.solutions/theory_seabed_3d_profile.html. / (accessed May 2022).
- Gobat, J., Grosenbaugh, M., 2001. Dynamics in the touchdown region of catenary moorings. *Int. J. Offshore Polar Eng.* **11**. URL: https://www.researchgate.net/publication/254509751_Dynamics_In_the_Touchdown_Region_of_Catenary_Moorings.
- Kelley, C., 2003. *Solving Nonlinear Equations with Newton's Method*. Fundamentals of Algorithms. ISBN 978-0-89871-546-0 doi:<https://doi.org/10.1137/1.9780898718898>.
- Kempener, R., Neumann, F., 2014. *IRENA Ocean Energy Technology Brief 4, Tech. rep.* [Consulta en 4-04-2022]. URL: <https://www.irena.org/publications/2014/Jun/Wave-energy>.
- Marques, F., Flores, P., Pimenta, J., Lankarani, H., 2016. A survey and comparison of several friction force models for dynamic analysis of multibody mechanical systems. 86, 1407–1443. doi:<https://doi.org/10.1007/s11071-016-2999-3>.
- Montano, A., Restelli, M., Sacco, R., 2007. Numerical simulation of tethered buoy dynamics using mixed finite elements. *Comput. Methods Appl. Mech. Eng.* **196**(41), pp. 4117–4129. doi:<https://doi.org/10.1016/j.cma.2007.04.012>.
- Orazi, L., Reggiani, B., 2020. A novel algorithm for a continuous and fast 3d projection of points on triangulated surfaces for CAM/CAD/CAE applications. *J. King Saud Univ. - Comput. Inf. Sci.* **34**(4), pp. 9–22. doi:<https://doi.org/10.1016/j.jksuci.2020.06.005>.

- Orcaflex, 1987-2022. Environment: Seabed data. URL: <https://www.orcina.com/webhelp/OrcaFlex/Default.htm>. / (accessed May 2022).
- Palm, J., Eskilsson, C., Bergdahl, L., 2017. An hp-adaptive discontinuous Galerkin method for modelling snap loads in mooring cables. *Ocean Eng.* **144**, pp. 266–276. doi:<https://doi.org/10.1016/j.oceaneng.2017.08.041>.
- Palm, J., Paredes, G., Eskilsson, C. and Taveira-Pinto, F., Bergdahl, L., 2013. Simulation of mooring cable dynamics using a discontinuous Galerkin method. *Proceedings of the V International Conference on Computational Methods in Marine Engineering, 29-31 May, 2013, CIMNE, Hamburg, Germany.* , pp. 455–466. URL: https://www.researchgate.net/publication/259174691_SIMULATION_OF_MOORING_CABLE_DYNAMICS_USING_A_DISCONTINUOUS_GALERKIN_METHOD.
- ProteusDS, 2018. Manual. URL: <https://dsaocean.com/downloads/documentation/> (accessed May 2022).
- Rodríguez, A., Armesto, A., Guanche, R. and Barrera, C., Vidal, C., 2020. Simulation of marine towing cable dynamics using a finite elements method. *J.Mar. Sci. Eng.* **8**(2), pp. 140. doi:<https://doi.org/10.3390/jmse8020140>.
- Simmons, G., 1985. *Calculus with analytical geometry*. The McGraw-Hill companies. ISBN 0-07-057642-4 .
- Trubat, P., Molins, C., Gironella, X., 2020. Wave hydrodynamic forces over mooring lines on floating offshore wind turbines. *Ocean Eng.* **195**, 106730. doi:<https://doi.org/10.1016/j.oceaneng.2019.106730>.